JACS Au
AN OPEN ACCESS JOURNAL OF THE AMERICAN CHEMICAL SOCIETY

pubs.acs.org/jacsau

Article

Differential Contributions of Distinct Free Radical Peroxidation Mechanisms to the Induction of Ferroptosis

Quynh Do, Rutan Zhang, Gavin Hooper, and Libin Xu*

Cite This: *JACS Au* 2023, 3, 1100–1117

Read Online

ACCESS | Metrics & More | Article Recommendations | Supporting Information

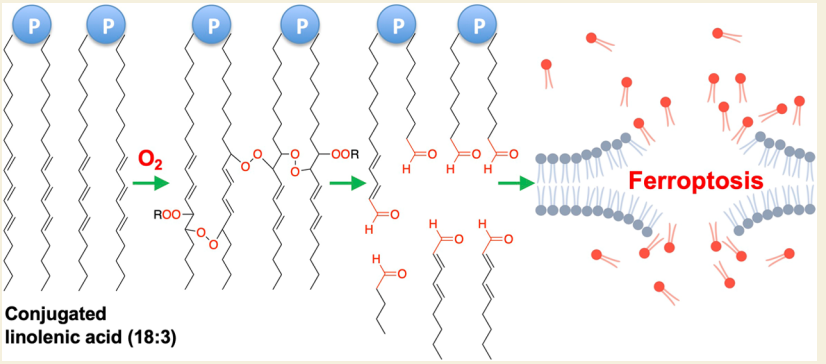

ABSTRACT: Ferroptosis is a form of regulated cell death driven by lipid peroxidation of polyunsaturated fatty acids (PUFAs). Lipid peroxidation can propagate through either the hydrogen-atom transfer (HAT) or peroxyl radical addition (PRA) mechanism. However, the contribution of the PRA mechanism to the induction of ferroptosis has not been studied. In this study, we aim to elucidate the relationship between the reactivity and mechanisms of lipid peroxidation and ferroptosis induction. We found that while some peroxidation-reactive lipids, such as 7-dehydrocholesterol, vitamins D_3 and A, and coenzyme Q10, suppress ferroptosis, both nonconjugated and conjugated PUFAs enhanced cell death induced by RSL3, a ferroptosis inducer. Importantly, we found that conjugated PUFAs, including conjugated linolenic acid (CLA 18:3) and conjugated linoleic acid (CLA 18:2), can induce or potentiate ferroptosis much more potently than nonconjugated PUFAs. We next sought to elucidate the mechanism underlying the different ferroptosis-inducing potency of conjugated and nonconjugated PUFAs. Lipidomics revealed that conjugated and nonconjugated PUFAs are incorporated into distinct cellular lipid species. The different peroxidation mechanisms predict the formation of higher levels of reactive electrophilic aldehydes from conjugated PUFAs than nonconjugated PUFAs, which was confirmed by aldehyde-trapping and mass spectrometry. RNA sequencing revealed that protein processing in the endoplasmic reticulum and proteasome are among the most significantly upregulated pathways in cells treated with CLA 18:3, suggesting increased ER stress and activation of unfolded protein response. These results suggest that protein damage by lipid electrophiles is a key step in ferroptosis.

KEYWORDS: *conjugated polyunsaturated fatty acids, lipid peroxidation, peroxyl radical addition, ferroptosis, lipid electrophiles, unfolded protein response, ER stress*

INTRODUCTION

Molecular oxygen is essential for cellular metabolism and energy production. However, the accumulation of reactive oxygen species (ROS) resulting from the imbalance between pro-oxidative and antioxidative processes can lead to oxidative stress in cells. Oxidative stress results in various deleterious effects, such as damage to macromolecules like DNA, proteins, and lipids.[1] The attack of ROS on lipids, termed lipid peroxidation, leads to free radical chain reactions with molecular oxygen.[2] Lipid peroxidation has been found to be implicated in multiple pathologies, such as diabetes,[3] cancer,[4,5] aging,[6] and neurodegenerative diseases.[7,8]

The autoxidation mechanism includes three steps: initiation, propagation, and termination (Figure 1a).[2] During the rate-limiting propagation step, the peroxyl radical can undergo the hydrogen (H)-atom transfer (HAT) mechanism to abstract the H atom from another lipid substrate to form lipid hydroperoxides. In addition, the peroxyl radical can undergo the peroxyl radical addition (PRA) mechanism and react with the "C═C" double bond of another lipid. The radical formed from

Received: December 12, 2022
Revised: February 14, 2023
Accepted: February 14, 2023
Published: March 4, 2023

https://doi.org/10.1021/jacsau.2c00681
JACS Au 2023, 3, 1100–1117

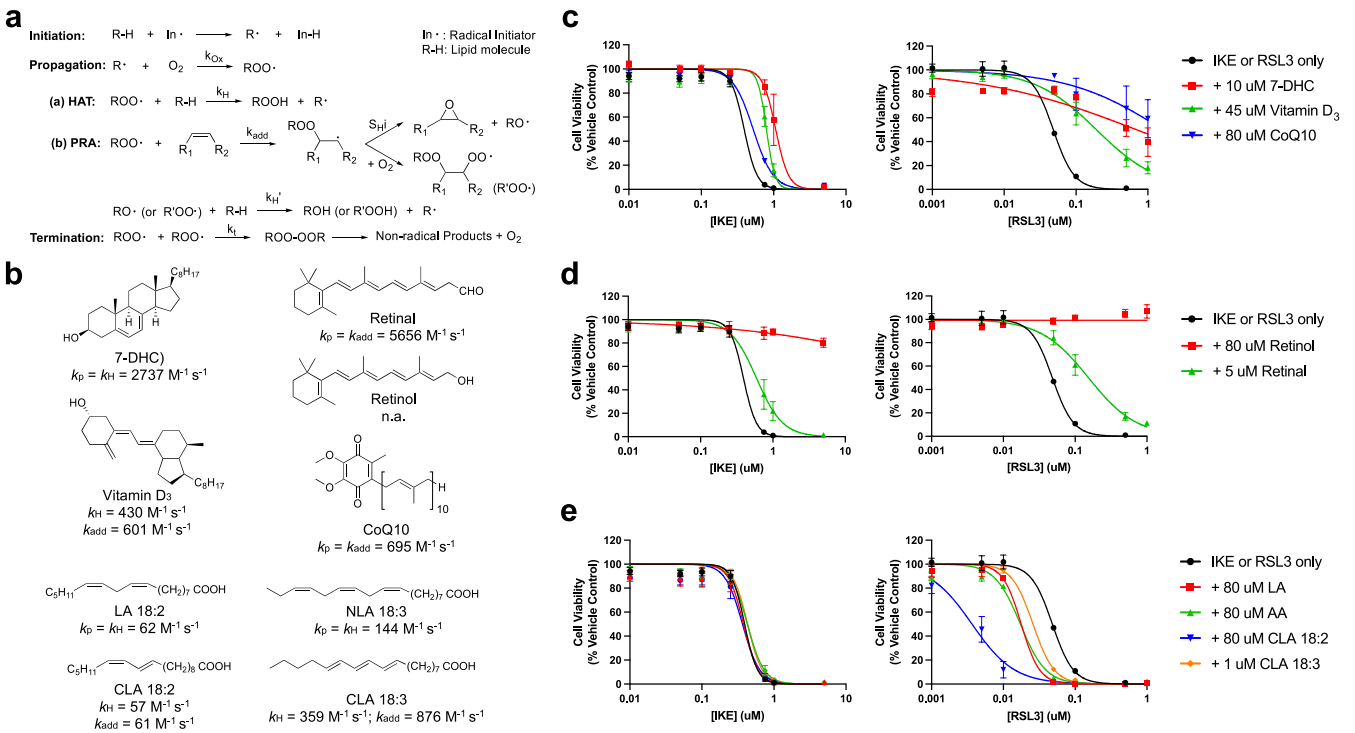

Figure 1. Various biologically important lipids can modulate the sensitivity of HT-1080 cell line to ferroptosis induced by IKE and RSL3. (a) Autoxidation mechanism of lipid peroxidation; (b) selected lipid structures in this study and their rate constants; (c–e) cell viability dose–response curves of HT-1080 cells treated with ferroptosis inducers, including imidazole ketone erastin (IKE) and RSL3, in the absence and presence of lipids shown in (b). Viability is plotted as mean ± SEM of n = 3 biological replicates.

this reaction can either undergo homolytic substitution (S_Hi) to form an epoxide or react with another molecular oxygen resulting in another peroxyl radical. The mechanism by which a lipid undergoes lipid peroxidation affects its oxidation product distribution and, thus, its biological effects.[9−11] For example, nonconjugated polyunsaturated fatty acids (PUFAs), such as linoleic and arachidonic acid, undergo the HAT reaction predominantly. Therefore, they would primarily form the HAT oxidation products such as lipid hydroperoxides and their degradation products, including 4-hydroxynonenal (4-HNE) and malondialdehyde.[2,12] These reactive electrophiles can react with the protein and DNA nucleophiles leading to defects in cellular processes.[11,13] Therefore, the elucidation of the autoxidation mechanism of different lipids would allow for a better understanding of their biological effects.

We recently reported a new radical clock approach that enabled us to distinguish and measure the rate constants of the HAT and PRA mechanisms of various biologically important lipids for the first time.[14] We found that lipid species with conjugated double bonds in their structure, such as coenzyme Q10 (CoQ10) and the lipophilic vitamins, vitamins A and D_3, have significant contributions from the PRA mechanism to the overall rate constant and, thus, are highly reactive toward lipid peroxidation. Importantly, we discovered that while the nonconjugated PUFAs only undergo the HAT mechanism, the conjugated ones can undergo both HAT and PRA mechanisms, with a predominant contribution from the latter for those with three or more double bonds. In addition, the conjugated PUFAs are much more reactive toward lipid peroxidation than their nonconjugated counterparts. Particularly, conjugated linolenic acid (CLA 18:3) has a much higher peroxidation rate constant (k_p = 1235 M^{-1} s^{-1}) compared to those of the nonconjugated PUFAs with even more double bonds, including AA (20:4) (k_p = 197 M^{-1} s^{-1}), eicosapentaenoic acid (EPA; 20:5) (k_p = 249 M^{-1} s^{-1}), and docosahexaenoic acid (DHA; 22:6) (k_p = 334 M^{-1} s^{-1}) (Figures 1b and S1). While the oxidation product profiles and the biological effects of nonconjugated PUFAs have been studied intensively, those of conjugated PUFAs are not well characterized. Therefore, in this paper, we investigated the oxidation product profiles of conjugated PUFAs with a focus on their implications in ferroptosis.

Ferroptosis, also known as cell death by lipid peroxidation, is a regulated form of cell death that is morphologically, biochemically, and genetically distinct from other types of cell death, such as apoptosis, necrosis, and autophagy.[15−17] Specifically, due to their special metabolic needs to support rapid differentiation and proliferation, certain cancer cell lines are constantly under high levels of oxidative stress, resulting in a high level of lipid peroxidation.[5,18] Therefore, these cells rely heavily on the activities of the antioxidant network, especially those that can function at the lipid membrane, such as the enzyme glutathione peroxidase (GPX4)[19−21] and ferroptosis suppressor protein 1 (FSP1),[22,23] for their survival. Thus, ferroptosis small-molecule inducers, such as RSL3 and erastin, which are direct and indirect inhibitors of GPX4, respectively, can lead to the accumulation of toxic lipid oxidation products and, subsequently, cell death.[15,19,24]

Despite the establishment of several key aspects of ferroptosis throughout the ten years since its discovery, certain questions remained unanswered,[17,25] such as the key molecular events between lipid peroxidation and the eventual cell death. Specifically, even though the autoxidation of PUFAs-containing phospholipid in the cellular membrane has been established to be the driver of ferroptosis,[25−28] it remains unknown whether the accumulation of oxidation products can

https://doi.org/10.1021/jacsau.2c00681
JACS Au 2023, 3, 1100−1117

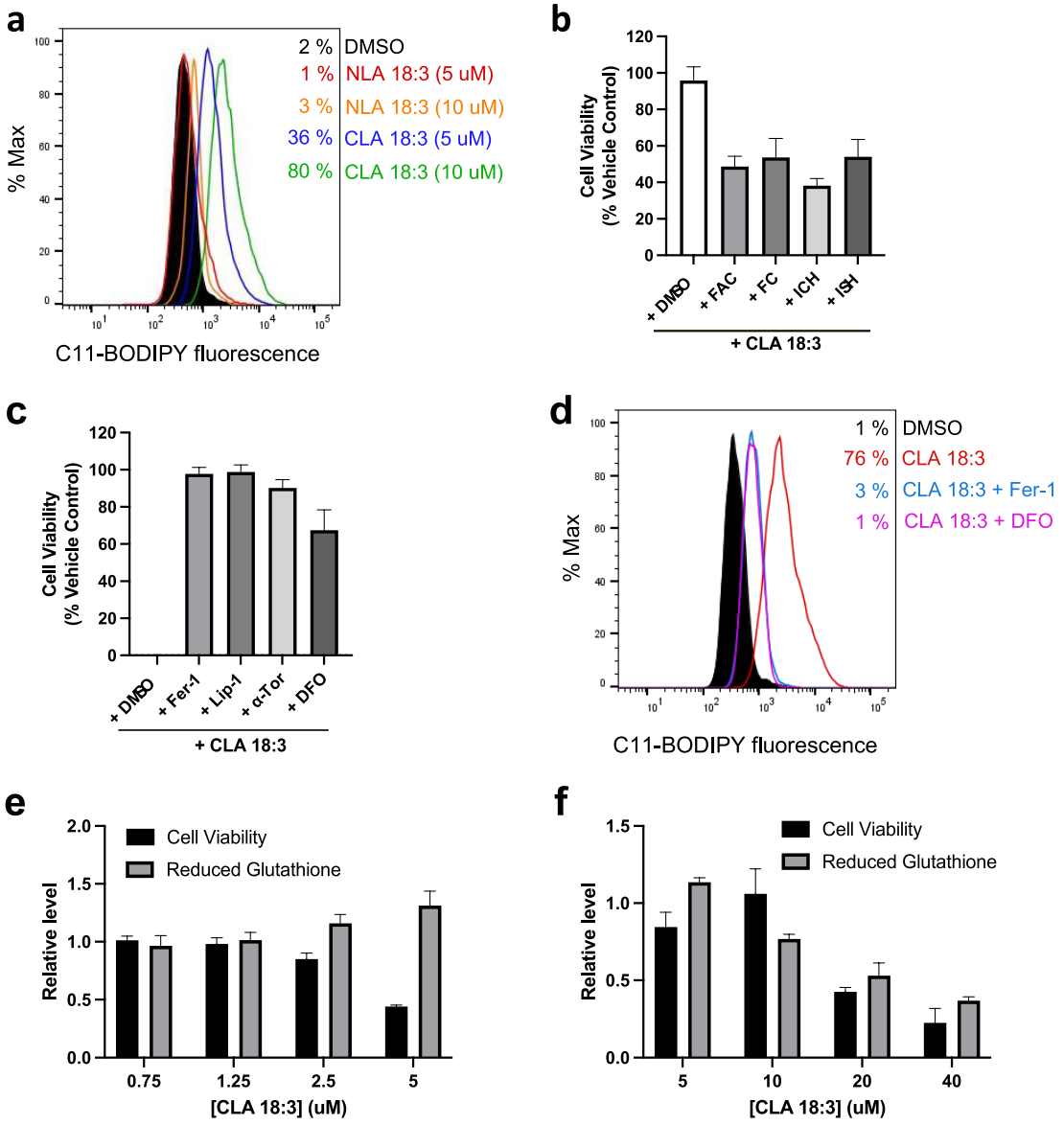

Figure 2. CLA 18:3 can induce ferroptosis as a single agent without affecting the level of cellular reduced glutathione in HT-1080 cell line. (a) Lipid peroxidation level after 5 h of treatments with 5 and 10 μM NLA 18:3 and CLA 18:3 assayed by flow cytometry using C11-BODIPY. (b) Cell viability after 3 h of treatment with 10 μM CLA 18:3 ± ferric ammonium citrate (FAC, 38 μM), ferric citrate (FC, 25 μM), iron chloride hexahydrate (ICH, 25 μM), and iron sulfate heptahydrate (ISH, 25 μM). Viability is plotted as mean ± SD of n = 3 biological replicates. (c) Cell viability after 24 h of treatment with 10 μM CLA 18:3 ± ferrostatin-1 (Fer-1, 1 μM), liproxstatin-1 (Lip-1, 1 μM), α-tocopherol (α-Tor, 100 μM), and deferoxamine (DFO, 80 μM). Viability is plotted as mean ± SD of n = 3 biological replicates. (d) Lipid peroxidation level after 5 h of treatments with 10 μM CLA 18:3 in the absence and presence of Fer-1 (1 μM) or DFO (80 μM) assayed by flow cytometry using C11-BODIPY. (e) Relative viability and level of reduced glutathione after 24 h of treatments with 0.75, 1.25, 2.5, and 5 μM CLA 18:3. Relative level is plotted as mean ± SD of n = 3 technical replicates. (f) Relative viability and level of reduced glutathione after 3 h treatment with 5, 10, 20, and 40 μM CLA 18:3. Relative level is plotted as mean ± SD of n = 3 technical replicates.

lead to membrane, protein, and DNA damage and if any of these events are responsible for the point of no-return in ferroptosis. In addition, while the relevance of nonconjugated PUFAs and their HAT oxidation products, such as lipid hydroperoxides, in ferroptosis, have been studied intensively,[16,24,29,30] the contribution of the PRA mechanism and its oxidation products to ferroptosis have not been characterized. The high autoxidation reactivity of conjugated PUFAs, which predominantly undergo the PRA reaction, suggests these lipids' potential to induce ferroptosis. Indeed, CLA 18:3 isomers, including α-eleostearic and pucinic acid, were recently reported to induce cell death in triple-negative breast cancer and carcinoma cell line, respectively.[31,32] Interestingly, cytotoxicity of conjugated PUFAs in cancer cells was reported even before the discovery of ferroptosis.[33−36]

In this work, we first investigated the effects of various biologically important lipids on ferroptosis induction in cancer cell lines and found that some lipids act as inhibitors and that conjugated polyunsaturated fatty acids (PUFAs) can induce or potentiate ferroptosis much more potently than nonconjugated PUFAs. We confirmed the incorporation of nonconjugated and conjugated PUFAs into membrane lipids, but different lipid classes. Next, based on the proposed autoxidation mechanism

https://doi.org/10.1021/jacsau.2c00681
JACS Au 2023, 3, 1100−1117

of conjugated PUFAs, we detected the highly electrophilic aldehydes formed from the PRA mechanism of conjugated PUFAs. Last, we investigated the cytotoxicity of the lipid-derived electrophiles and their lethal mechanism via RNA sequencing, which suggested that protein damage is one of the key steps in conjugated PUFA-induced ferroptosis. Here, the examination of the lethal mechanism of conjugated PUFAs highlights the underappreciated contribution of the PRA mechanism and its oxidation products to ferroptosis.

RESULTS

Various Biologically Important Lipids Can Modulate the Sensitivity of Cancer Cells to Ferroptosis

Here, we carried out a systematic examination of the extent to which various biologically important lipids sensitize cells to cell death in the ferroptosis-sensitive cancer cell lines, including fibrosarcoma HT-1080, brain neuroblastoma SK-N-SH, and clear-cell renal carcinoma 786-O.[15,37,38] We first determined the cytotoxicity of the various lipids with rate constants measured in our previous study (Figures 1b and S1).[14] These lipids are 7-hydrocholesterol (7-DHC); CoQ10; vitamin D_3; the two forms of vitamin A, including retinol and retinal; the nonconjugated PUFAs, including linoleic acid (LA), nonconjugated linolenic acid (NLA 18:3), AA, EPA, and DHA; and the conjugated PUFAs, including the conjugated linoleic acid (CLA 18:2) and CLA 18:3. Retinoic acid, another form of vitamin A, was not examined in this study due to its low solubility in vehicle solvent. We found that 7-DHC, vitamin D_3, and retinal were particularly toxic in all three cell lines (Table S1). The toxicity of these lipids may be related to their high reactivity toward lipid peroxidation and the formation of oxidation products (Figures 1b and S1).[14] For example, oxysterols formed from the oxidation of 7-DHC are highly toxic to neuronal cells.[39−42] However, further investigation is needed to determine whether their toxicity is related to ferroptosis. In addition, the higher toxicity of retinal compared to retinol may be attributed to its aldehyde moiety. Notably, compared to other PUFAs, CLA 18:3 displayed much lower EC_{50} values of 4, 10, and 14 μM in the HT-1080, SK-N-SH, and 786-O cell lines, respectively (Table S1).

Next, we treated the cell lines with the two ferroptosis inducers imidazole ketone erastin (IKE) and RSL3 in the absence and presence of different lipid species at their nonlethal concentrations. The nonlethal concentration chosen for most lipids was 80 μM, but for the more toxic 7-DHC, vitamin D_3, and retinal, 10, 45, and 5 μM were used, respectively. In addition, CLA 18:3 was used at 1, 5, and 5 μM in the HT-1080, SK-N-SH, and 786-O cell lines, respectively. The EC_{50} values of the lipid-treated cells were then compared to the controls, which were treated with the inducers only, to elucidate whether each lipid potentiates or inhibits ferroptosis. Overall, we observed similar trends among the cell lines for each lipid (Table S2). First, cell death induced by RSL3 was more sensitive to the addition of exogenous lipids than IKE (Figures 1c−e, S2, and S3). In addition, CoQ10 was found to suppress ferroptosis, which is consistent with its established properties as an antioxidant and a ferroptosis inhibitor (Figure 1c).[22,23,43] Interestingly, despite being more toxic than other lipids, when used at nonlethal concentrations, 7-DHC, vitamin D_3, and retinal potently inhibited RSL3-induced ferroptosis (Figure 1c, d). Moreover, between the two forms of vitamin A, retinol was more potent in inhibiting ferroptosis than retinal, which may be because 80 μM retinol was used while the retinal concentration was 5 μM (Figure 1d).

We also found that cell death was inhibited across the three cell lines when the cells were cotreated with the monounsaturated fatty acid OA (Table S2). This result is consistent with the previous findings that OA is a potent ferroptosis suppressor.[24,44] Among the nonconjugated PUFAs, AA was the most potent in enhancing ferroptosis in all three cancer cell lines. We also observed that the ω-6 fatty acids, including LA and AA, could sensitize cell death induced by IKE and RSL3 more potently than the ω-3 fatty acids, including EPA and DHA (Table S2). Importantly, we found that the conjugated PUFAs were much more potent than the nonconjugated ones in potentiating ferroptosis (Figure 1e). For example, CLA 18:2 led to a 13-fold increase in RSL3-induced toxicity (EC_{50} = 3.7 nM) in the HT-1080 cell line (Table S2) while LA led to only a 3-fold increase in RSL3 lethality (EC_{50} = 18 nM). CLA 18:3 (EC_{50} = 36 nM) could also sensitize cells to ferroptosis but at a concentration 80 times lower than the concentration used for other PUFAs.

CLA 18:3 Induces Ferroptosis within Cellular Membranes

Due to the high toxicity of CLA 18:3 in all three cancer cell lines, we next investigated whether CLA 18:3 induced ferroptosis in the HT-1080 cell line. First, we found that treating the cells with CLA 18:3 led to a dose-dependent accumulation of lipid peroxidation as assayed by flow cytometry using the fluorescent probe C11-BODIPY (Figure 2a). In contrast, the addition of the nonconjugated isomer, NLA 18:3, did not lead to changes in the lipid peroxidation level compared to the control (Figure 2a). Next, we confirmed that cell death induced by CLA 18:3 can be sensitized by the addition of different iron sources (Figure 2b). Last, we determined that CLA 18:3-induced death can be inhibited by the ferroptosis inhibitors, including radical-trapping antioxidants ferrostatin-1 (Fer-1), liproxstatin-1 (Lip-1), and α-tocopherol (α-Tor), and the iron chelator deferoxamine (DFO) (Figure 2c). Moreover, the addition of either Fer-1 or DFO can reduce the lipid peroxidation level of CLA 18:3-treated cells to the same level of the control (Figure 2d). These data suggest that CLA 18:3 induced ferroptosis in the HT-1080 cell line as a single agent.

Previously, α-eleostearic acid, a CLA 18:3 isomer, was reported to induce ferroptosis without inhibiting the function of GPX4 or affecting the cellular total glutathione level.[31] Therefore, we next sought to determine whether the treatment with CLA 18:3 could lead to changes in the level of reduced glutathione. Reduced glutathione functions as a free radical scavenger, and a decrease in the ratio of the reduced to the oxidized form indicates an increase in cellular oxidative stress.[45−47] Therefore, we postulated that even though the level of total cellular glutathione is not affected, the increased oxidative stress induced by CLA 18:3 can potentially lead to a decrease in the reduced glutathione level. However, we found that the reduced glutathione level was unaffected despite the decrease in cell viability upon treatment with 2.5 and 5 μM CLA 18:3 (Figure 2e). Furthermore, we only observed the reduction in reduced glutathione level when cells were treated with CLA 18:3 at the high concentrations of 10, 20, and 40 μM (Figure 2f). These results suggest that CLA 18:3-induced lethal effects happen within the cellular lipid membrane since glutathione is water-soluble and cannot scavenge free radicals within the lipid bilayer.

https://doi.org/10.1021/jacsau.2c00681
JACS Au 2023, 3, 1100−1117

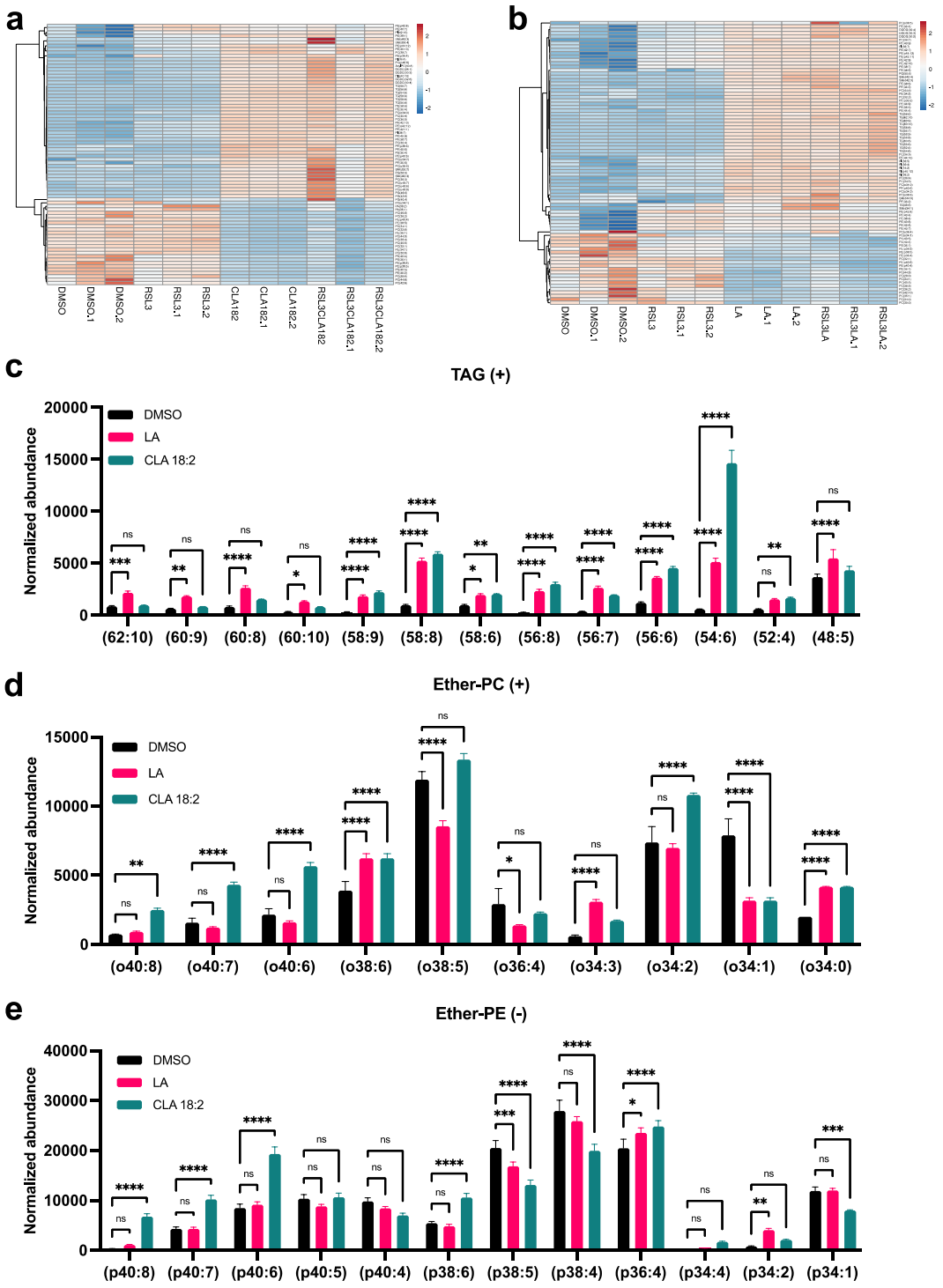

Figure 3. Untargeted lipidomics reveals distinct changes associated with the addition of nonconjugated and conjugated PUFAs in HT-1080 cell line. Heat map of significantly altered lipid species in the positive mode upon the addition of (a) CLA 18:2 and (b) LA with or without RSL3 cotreatment for 24 h. Normalized abundance of (c) TAG, and (d) ether-PC lipids in the positive mode, and (e) ether-PE lipids in the negative mode across specified treatments for 24 h. *p*-Values from Student's *t*-test against control with Bonferroni correction for multiple comparisons are shown; ns = nonsignificant, $*p < 0.032$, $**p < 0.0021$, $***p < 0.0002$, $****p < 0.0001$. TAG = triacylglycerol, ether-PC = ether-linked phosphatidylcholine, ether-PE = ether-linked phosphatidylethanolamine. Concentrations of RSL3, LA, CLA 18:2 are 0.005, 80, and 80 μM, respectively. Normalized abundance is plotted as mean ± SD of $n = 3$ biological replicates for each condition.

Nonconjugated and Conjugated PUFAs are Incorporated into Distinct Cellular Lipid Species

To provide insights into the mechanisms underlying the difference in ferroptosis-sensitizing potency of nonconjugated and conjugated PUFAs, we first performed untargeted lipidomic analysis using our established HILIC-ion mobility-mass spectrometry method[48,49] to assess the changes in the lipidome of the HT-1080 cell line upon the addition of RSL3, LA, CLA 18:2, or a combination of RSL3 with either LA (RSL3+LA) or CLA 18:2 (RSL3+CLA 18:2) relative to the

https://doi.org/10.1021/jacsau.2c00681
JACS Au 2023, 3, 1100−1117

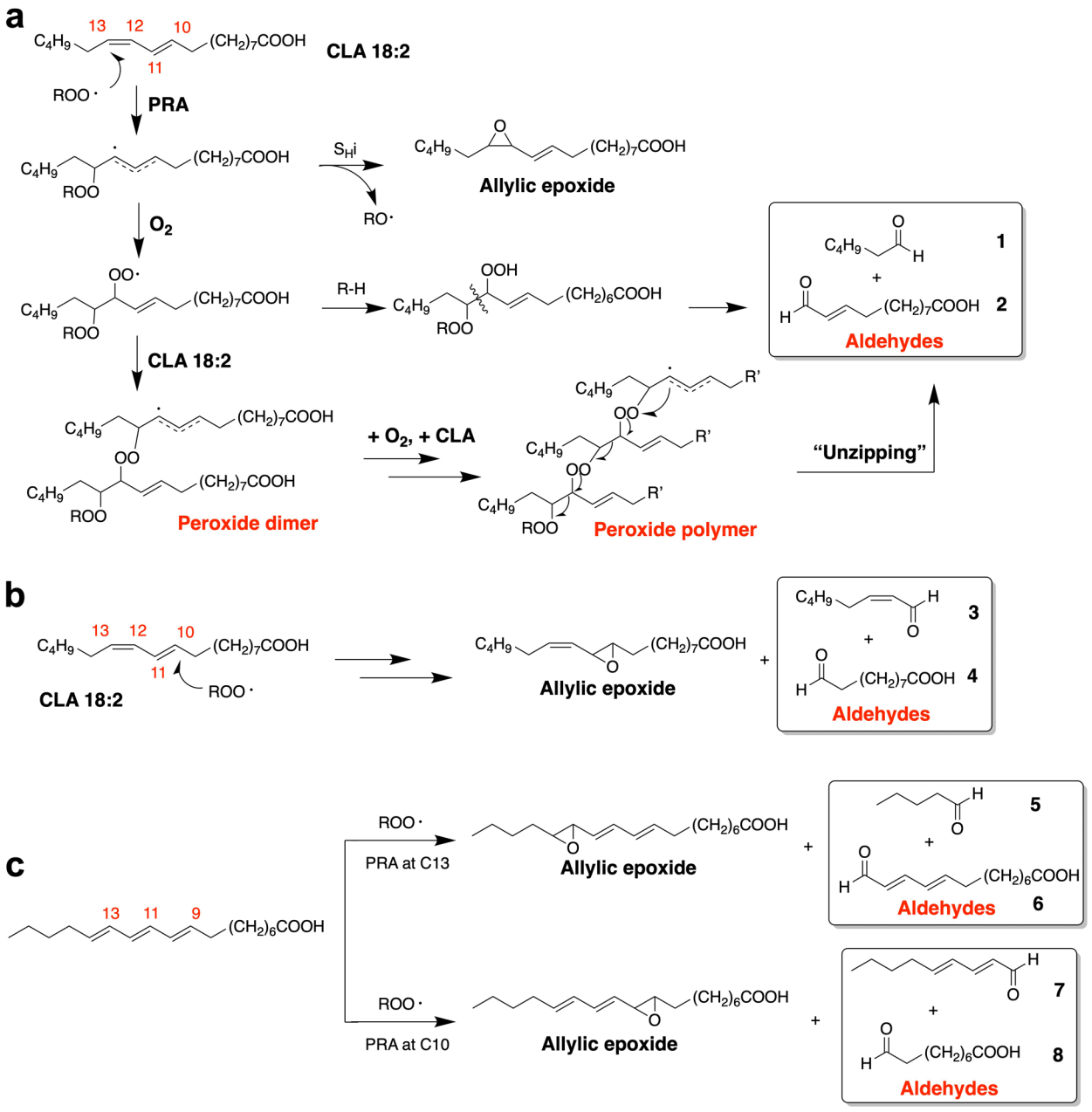

Figure 4. PRA mechanism of conjugated PUFAs leads to the formation of peroxide dimers and polymers, and, subsequently, electrophilic aldehydes. (a) Proposed PRA mechanism of CLA 18:2 at C13 leading to the formation of hexanal (**1**) and the *α,β*-unsaturated aldehyde 2. (b) Proposed oxidation product from PRA reaction at C10 of CLA 18:2 based on similar mechanism leading to the formation of 2-octenal (**3**) and the saturated aldehyde 4. (c) Proposed oxidation product from PRA reaction of CLA 18:3 based on similar mechanism leading to the formation of pentanal (**5**), the *α,β,δ,γ*-unsaturated (conjugated dienal) aldehyde **6**, 2,4-*tt*-nonadienal (7), and the saturated aldehyde **8**.

vehicle control. Principal component analysis showed separation in both positive and negative modes among three clusters: DMSO and RSL3, LA and RSL3+LA, and CLA 18:2 and RSL3+CLA 18:2 (Figure S4). Since the concentration used for RSL3 here was only 5 nM, its addition did not cause a significant difference in lipid composition in the treatment pairs, including RLS3 versus control, RSL3-LA versus LA, and RSL3+CLA 18:2 versus CLA 18:2.

Significantly altered lipid species (ANOVA adjusted p-value <0.05) between each treatment and the control were identified by m/z, retention time, and collision cross section (CCS) values using LiPydomics developed by our lab[50] (Table S3–S6). We found that adding LA and CLA 18:2 either by themselves or in combination with RSL3 led to significant changes compared with DMSO- or RSL3-treated cells (Figures 3a,b and S5a,b). In addition, in both CLA 18:2- and LA-treated groups, most of the altered lipids belong to two lipid classes: phosphatidylcholine (PC) and phosphatidylethanolamine (PE) (Table S3–6). Within these two classes, many long-chain and highly unsaturated lipids were found to be elevated, while there was a decrease in the abundance of shorter-chain and monounsaturated or saturated lipids (Figure S5c,d). Moreover, there was a significant increase in the abundance of triacylglyceride (TAG) species in both LA and CLA 18:2 treatments (Figure 3c).

https://doi.org/10.1021/jacsau.2c00681
JACS Au 2023, 3, 1100−1117

On the other hand, CLA 18:2-induced changes were significantly different from LA-induced changes in both positive and negative modes. Specifically, we found that the addition of exogenous CLA 18:2 induced a more drastic increase in the normalized lipid abundance compared to the control than the addition of LA. For example, in the negative mode, in CLA 18:2-treated cells, PC (40:8) and PE (p40:8) had the highest fold changes of 226 and 22.2, respectively, compared to the control (Table S3). In contrast, the highest fold changes found in LA-treated cells were only 5.2 and 4.2 for PE (p34:2) and DGDG (30:3), respectively (Table S5).

Furthermore, the addition of LA led to a moderate increase in very long-chain and highly unsaturated TAGs while CLA 18:2 treatment led to a significant increase in the levels of shorter-chain and less unsaturated TAGs, suggesting the involvement of distinct mechanisms in the incorporation of LA and CLA 18:2 into the cellular lipidome (Figure 3c, Tables S3 and S5). Notably, while TAG (54:6) was the most elevated TAG species in both LA- and CLA 18:2-treated cells, it was much more abundant in CLA 18:2-treated than LA-treated cells, with a fold change of 25.2 and 8.8, respectively. Fragmentation of this lipid in the positive mode confirmed the incorporation of CLA 18:2 into all three positions of TAG (54:6) (Figure S6a). Similarly, we also observed a significant elevation of PC (36:4) and PE (36:4) in CLA 18:2-treated compared to LA-treated cells (Figure S5c,d). Fragmentation of these lipids in the negative mode confirmed the incorporation of CLA 18:2 (Figure S6b,c, Table S9).

Interestingly, the addition of CLA 18:2, but not LA, was found to significantly increase the abundance of various long-chain and highly unsaturated ether-PC and ether-PE lipids compared to the control (Figure 3d, e). Strikingly, we observed that the significantly increased ether-PEs, including PE (p40:8), PE (p40:7), and PE (p40:6), consisted of fatty acid 18:2 at the *sn*-1 position and fatty acid 22:6, 22:5, and 22:4 at the *sn*-2 position, respectively (Figure S6d–f, Table S9). This observation is surprising since in endogenous plasmalogens, palmitic (16:0), stearic (18:0), and oleic (18:1) chains are almost exclusively incorporated in the *sn*-1 position, and the *sn*-2 position primarily consists of PUFAs.[51] Due to the pro-ferroptosis properties of ether phospholipids,[52,53] the more significant increase of these lipid species in CLA 18:2-treated samples can potentially contribute to the higher potency of CLA 18:2 in enhancing ferroptosis.

CLA 18:3 at 3 μM also led to changes in lipid composition relative to the control (Figure S7a,b). Similar to the treatment with CLA 18:2, we observed that most altered lipids were phospholipids and ether-lipids, especially ether-PEs (Tables S7 and S8). However, we found that not all highly increased lipids contain fatty acid 18:3 in their composition (Figure S7c,d, Table S9), which could be due to the low concentrations of CLA 18:3 used (3 μM vs 80 μM for CLA 18:2). Because 3 μM CLA 18:3 can induce cell death, the lipid composition changes in CLA 18:3-treated cells may reflect the changes in cells undergoing ferroptosis.

Electrophilic Lipid Aldehydes Are Formed from the PRA Mechanism of Conjugated PUFA and Are Toxic to the Cells

Nonconjugated and conjugated PUFAs undergo lipid peroxidation via distinct mechanisms.[14] For example, LA only undergoes the HAT mechanism to form products such as lipid hydroperoxide (HPODEs), including 9-*trans*,*cis*(*tc*)-, 9-*trans*,-*trans*(*tt*)-, 13-*tt*-, and 13-*tc*-HPODE (Figure S8a). However, based on the peroxidation kinetics of CLA 18:2,[14] we expect oxidation products from both HAT and PRA mechanisms. From the HAT mechanism, abstraction of the H atoms at either C9 or C14 positions would lead to the formation of 9-*tc*-, 10-*tt*-, 13-*tt*-, and 14-*tc*-HPODE (Figure S8b). Isomerization to 9-*tt*-HPODE and 14-*tt*-HPODE is also possible following the oxygen addition at C9 or C14, bond rotation, β-fragmentation, then oxygen addition process, similar to the mechanisms of LA oxidation.[54] To elucidate the oxidation products from CLA 18:2, we carried out free radical oxidation using 2,2′-Azobis(4-methoxy-2,4-dimethylvaleronitrile) (MeOAMVN) as the radical initiator, reduced the reaction mixture with triphenylphosphine, which would reduce the lipid hydroperoxides formed into corresponding alcohols (HODEs), and analyzed the products using normal phase HPLC-UV at 234 nm. Here, many more peaks were observed in the chromatogram of CLA 18:2 relative to that of LA, suggesting a much more complex mixture of products from the oxidation of conjugated PUFAs (Figure S9a). When the reaction mixture was reduced to dienyl diols (HODOLs) using $LiAlH_4$,[14] a much cleaner chromatogram was observed for CLA 18:2, and the retention times of 9-*tc*, 9-*tt*, 10-*tt*, 13-*tt*, 14-*tc*, and 14-*tt* peaks were tentatively assigned by comparing with the peaks found from LA oxidation (Figure S9b).

From the PRA mechanism, the carbon radical formed after PRA to C13 of CLA 18:2 can undergo homolytic substitution (S_Hi) to form an allylic epoxide (Figure 4a). However, we were not able to identify allylic epoxides from the oxidation of CLA 18:2, which could be because these products could not survive the reduction condition. The resulting carbon radical can also react with another molecular oxygen, leading to the formation of another peroxyl radical, which can produce a diperoxide lipid after abstracting an H atom or add to the double bond of another CLA 18:2 molecule leading to peroxide dimers and polymers (Figure 4a). The lipid dimers and polymers can then undergo "unzipping" reactions leading to the formation of the α,β-unsaturated aldehyde **1** and the saturated aldehyde **2**, which is hexanal. Such "unzipping" reactions have been well-studied using styrene-peroxide polymers.[2] Similarly, the PRA reaction at C10 of CLA 18:2 can lead to the formation of the saturated aldehyde **3** and the α,β-unsaturated aldehyde **4**, 2-octenal (Figure 4b). A similar PRA mechanism can also be applied to CLA 18:3, which suggests the formation of the saturated aldehyde pentanal (**5**) and the $\alpha,\beta,\delta,\gamma$-unsaturated aldehyde (termed conjugated dienal for short), 2,4-*tt*-nonadienal, as the major oxidation products (Figures 4c and S10a,b). Indeed, peroxide dimers and polymers have been previously identified as the major oxidation products of conjugated PUFAs, especially during the initial oxidation stage,[55−58] and volatile aldehyde compounds have also been detected in CLA 18:2-rich oil and purified TAGs,[59] supporting the proposed mechanisms here.

To elucidate the aldehydes formed from the oxidation of conjugated PUFAs, we carried out free radical oxidation of CLA 18:2, CLA 18:3, and CLA 18:3-rich tung oil in comparison with LA in benzene at 37 °C using MeOAMVN. While we used β-eleostearic acid as CLA 18:3 in this study, tung oil is composed of TAGs in which about 75% of the total acyl chains are esterified α-eleostearic acid.[35] Therefore, we used tung oil as the model for the oxidation of CLA 18:3-containing TAGs as well as to confirm the oxidation products from both isomers. To capture the volatile aldehydes, we purged the reaction vials with N_2 gas and captured the vapor

https://doi.org/10.1021/jacsau.2c00681
JACS Au 2023, 3, 1100−1117

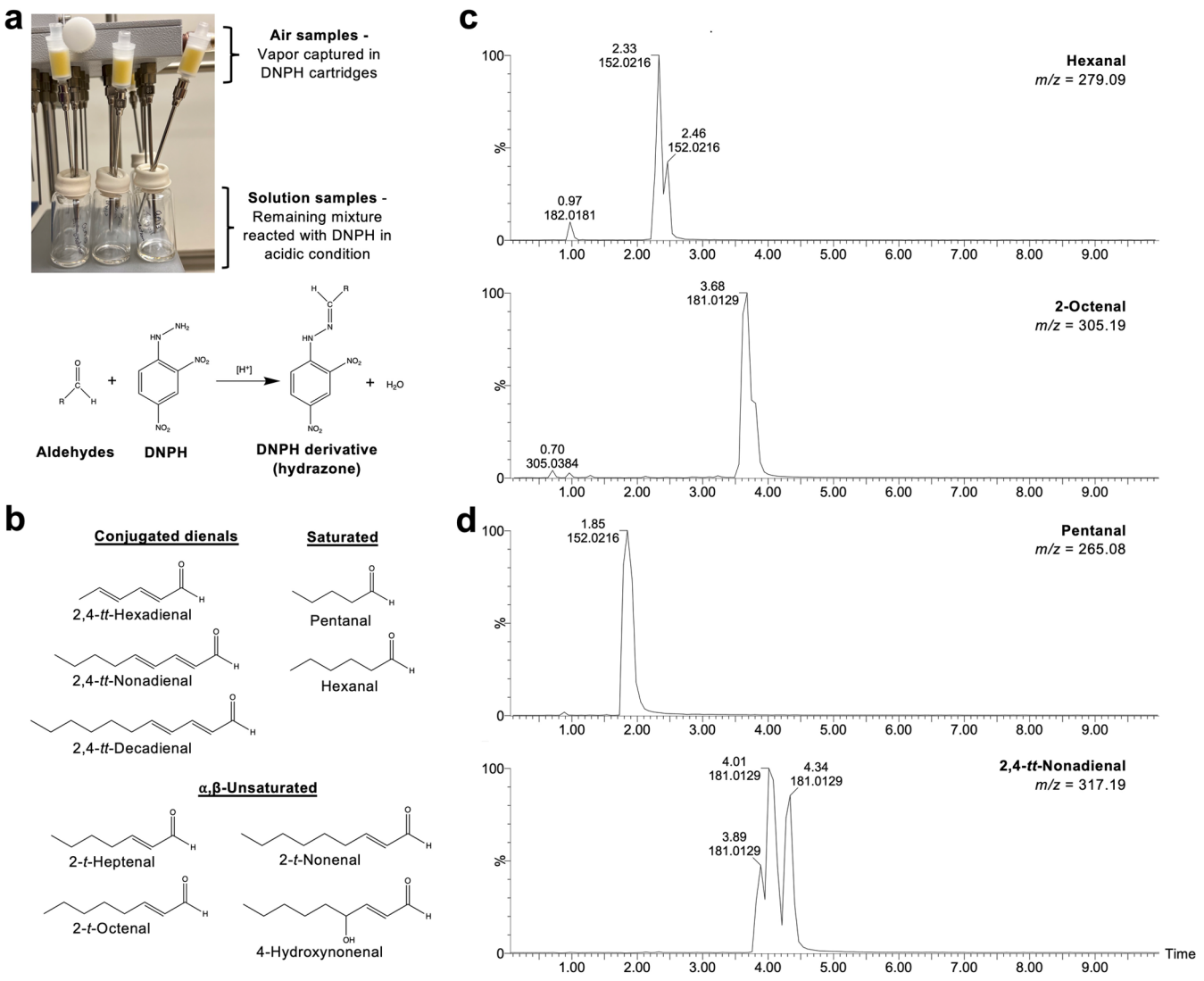

Figure 5. Volatile aldehydes can be detected from the oxidation of conjugated PUFAs. (a) Experimental setup to detect aldehydes from conjugated PUFA oxidation via derivatization using 2,4-dinitrophenylhydrazine (DNPH). DNPH-derivatized aldehydes from both the air and solution samples were extracted using CH_2Cl_2, evaporated, and reconstituted in reverse phase-LC solvent for MS analysis. (b) Structures of the aldehydes examined in this study. (c) MS chromatogram of hexanal and 2-octenal detected from the air sample of CLA 18:2. d) MS chromatogram of pentanal and 2,4-*tt*-nonadienal detected from the oxidation of CLA 18:3.

using cartridges containing 2,4-dinitrophenylhydrazine (DNPH), which derivatizes aldehydes to hydrazone, as described previously (Figure 5a).[60−62] The remaining mixtures in the vial were also treated with DNPH under acidic conditions. Then, both the DNPH-treated air (vapor) and solution (from the reaction vial) samples were analyzed using reverse-phase LC (RPLC)-MS and MS/MS fragmentation in the negative ion mode. The fragmentation spectra detected were compared to a series of aldehyde standards to confirm the identity of aldehydes formed from each oxidation mixture (Figure 5b).

Overall, we observed that the air samples gave much cleaner total ion chromatograms compared to the solution ones. From the air samples of CLA 18:2 and CLA 18:3 (Figure S11), we detected hexanal and 2-octenal (Figure 5c) as well as pentanal and 2,4-*tt*-hexadienal (Figure 5d), which are the predicted oxidation products from the PRA mechanism of CLA 18:2 and CLA 18:3, respectively (Figure 4). The fragmentation patterns of these aldehydes matched those prepared from the commercially available aldehyde standard (note: 2-*t*-octenal, instead of 2-*c*-octenal, was used as the standard), confirming their identities (Figures S12 and S13). In addition, we found that both CLA 18:3 and tung oil oxidation led to the formation of 2,4-*tt*-hexadienal and the *α,β*−unsaturated aldehyde 2-*t*-heptenal while the levels of 2-octenal, 2-*t*-nonenal, and 4-HNE detected were negligible (Figure S14a,b). These results suggest that similar volatile aldehydes are formed in the oxidation of both free and TAG-incorporated CLA 18:3 as well as in both CLA 18:3 isomers.

Like CLA 18:2, the oxidation of LA also led to the formation of 2-octenal, as well as other *α,β*-unsaturated aldehydes, including 2-*t*-heptenal and 4-HNE (Figure S14c,d). Interestingly, in the air samples, while 2-*t*-nonenal was detected from the oxidation of CLA 18:2, the level of this aldehyde in the oxidation of LA is negligible (Figure S14c,d). We then roughly compared the level of each aldehyde from the oxidation of CLA 18:2 versus LA by comparing the total area under the curve from both air and solution samples of the aldehyde

https://doi.org/10.1021/jacsau.2c00681
JACS Au 2023, 3, 1100−1117

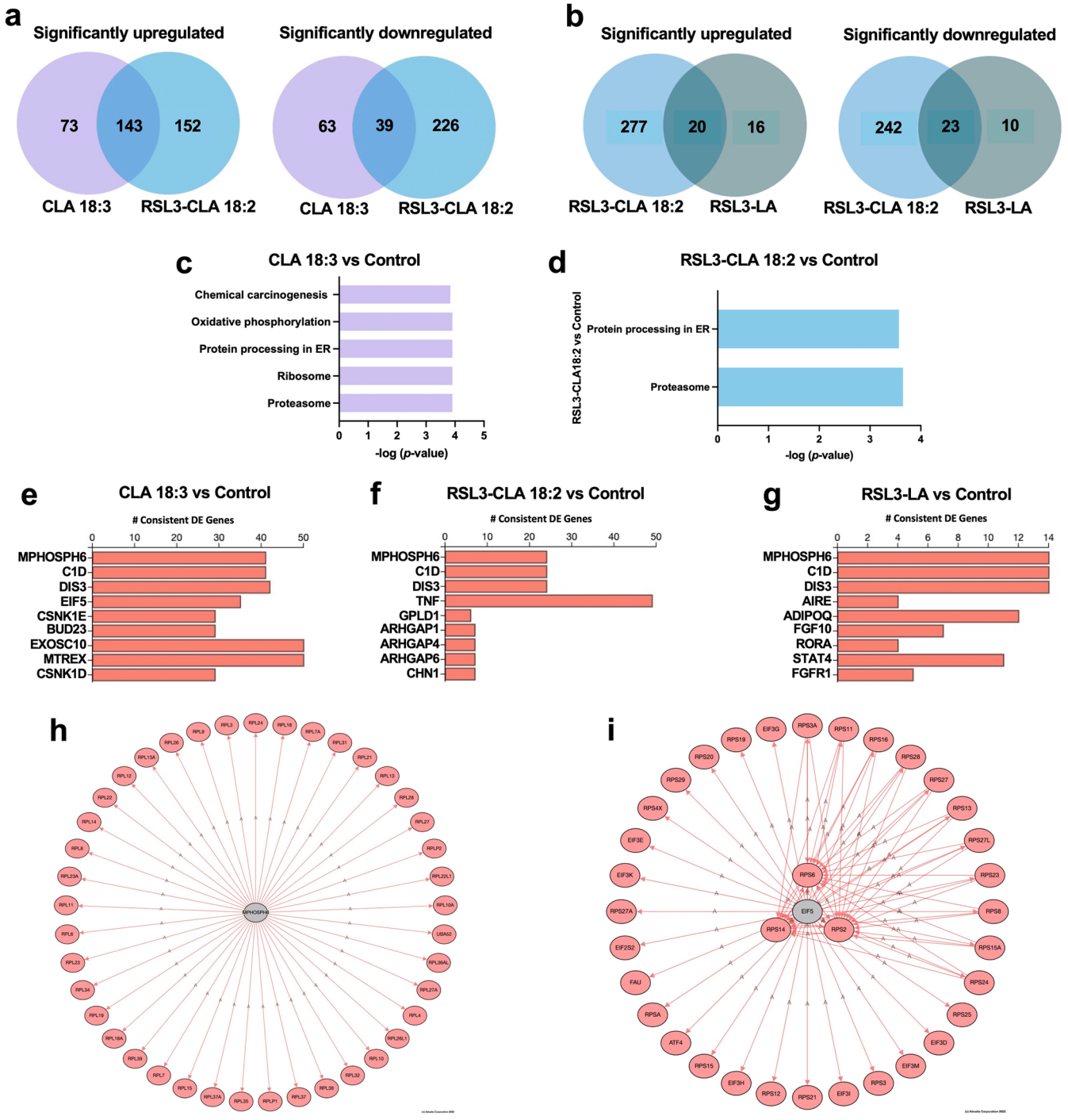

Figure 6. RNA sequencing data revealed that the addition of conjugated PUFAs can lead to increased protein damage in HT-1080 cell line. Venn diagram of genes commonly or uniquely up- and downregulated in cells treated with (a) CLA 18:3 and RSL3-CLA 18:2, and (b) RSL3-CLA 18:2 and RSL3-LA compared to the control (adjusted p-value < 0.05, >2-fold change). Top significantly upregulated pathways identified by Integrated Differential Expression and Pathway (iDEP) and iPathwayGuide (iPG) analyses in cells treated with (c) CLA 18:3 and (d) RSL3-CLA 18:2 compared to control (the −log(p-value) from iPG are shown, FDR-corrected). Top significantly activated upstream regulators identified iPathwayGuide (iPG) analysis in cells treated with (e) CLA 18:3, (f) RSL3-CLA 18:2, and (g) RSL3-LA compared to control (combined p-value < 0.05). DEGs regulated by the upstream regulators (h) M-phase protein 6 (MPHOSPH6) and (i) eukaryotic translation initiation factor-5 (EIF5) in cells treated with CLA 18:3 compared to control (adjusted p-value <0.05). n = 4 biological replicates per condition. Cells were treated for 24 h, and the concentrations used for CLA 18:3, CLA 18:2, LA, and RSL3 were 5, 80, 80, and 0.01 μM, respectively.

peaks. We found that while the levels of the saturated aldehydes, including pentanal and hexanal, were comparable between LA and CLA 18:2 oxidation, the levels of the α,β-unsaturated aldehydes were significantly different between the two groups. Specifically, 4-HNE, which has been established as the most abundant aldehyde product from the oxidation of ω-6 nonconjugated PUFAs,[2,63] was detected at a higher level in LA oxidation compared to CLA 18:2 oxidation while the levels of 2-t-heptenal, 2-octenal, and 2-t-nonenal were higher in CLA 18:2 compared to LA (Table S10). It is difficult to

https://doi.org/10.1021/jacsau.2c00681
JACS Au 2023, 3, 1100−1117

quantitatively compare the levels of aldehydes formation from CLA 18:2 and CLA 18:3 since different aldehydes are formed, but if we assume the aldehyde-DNPH adducts gave similar responses in mass spectrometry analysis, we found that the levels of 2,4-*tt*-nonadienal and pentanal formed from CLA 18:3 are 1.35- and 1.7-fold of those of 2-octenal and hexanal, respectively, formed from CLA 18:2 under the same condition (Table S11).

We next sought to compare the cytotoxicity of the aldehydes in HT-1080 cells. The unsaturated aldehydes are highly reactive electrophiles that can readily form adducts with nucleophiles. As expected, we found that the unsaturated aldehydes were much more toxic to the cells than the saturated ones (Table S12). In addition, the conjugated dienals were more toxic than the α,β−unsaturated ones with the same alkyl chain length; for example, 2,4-*tt*-nonadienal (EC_{50} = 13 μM) vs 2-*t*-nonenal (EC_{50} = 25 μM). Importantly, we found that 2,4-*tt*-nonadienal was as toxic to the cells as 4-HNE, which is known for its high cytotoxicity and implications in various pathologies.[63,64] Thus, the formation of 2,4-*tt*-nonadienal from the PRA reaction of CLA 18:3 can potentially contribute to the high toxicity of this fatty acid.

The Addition of Exogenous Conjugated PUFAs Leads to Increased Protein Damage and ER Stress

To elucidate the mechanism underlying the lethality of conjugated PUFAs, we carried out RNA sequencing (RNA-seq) to investigate transcriptomic changes in treatments with either CLA 18:3 or RSL3+CLA 18:2 compared with vehicle controls and cells treated with RSL3+LA (see Tables S18−S20 in Excel for complete lists of genes). We chose to compare these conditions because LA or CLA 18:2 alone does not induce cell death at the concentration (80 μM) used. Overall, compared with the control, the addition of CLA 18:3 and RSL3-CLA 18:2 led to 318 and 560 differentially expressed genes (DEGs), respectively (adjusted *p*-value <0.05, > 2-fold change) (Figure 6a). While CLA 18:3 upregulated 216 genes and downregulated 102 genes, RSL3-CLA 18:2 upregulated 295 genes and downregulated 265 genes. Among the DEGs, 182 genes were coregulated by both CLA 18:3 and RSL3-CLA 18:2, and 136 and 378 genes were uniquely regulated by CLA 18:3 and RSL3-CLA 18:2, respectively. Among the commonly upregulated genes by CLA 18:3 and RSL3-CLA 18:2, *DDIT4*, *HMOX1*, *SLC7A11*, *FTH1*, *FTL1*, and *GCLM* were previously found to associate with ferroptosis.[37,65,66]

To carry out pathway analyses of DEGs in the CLA 18:3 versus control comparison, we utilized the integrated Differential Expression and Pathway (iDEP) web application and iPathwayGuide (iPG) software.[67,68] Only pathways that are identified to be significantly altered by both tools are reported. For the pathway analysis module in iDEP, the thresholds for gene significance were set as FDR < 0.05 and >2 fold-change, and we chose the GAGE analysis method with pathway significance cutoff at 0.05 (FDR < 0.05).[69] Using both methods, we identified proteasome, ribosome, and protein processing in endoplasmic reticulum (ER) among the top significantly activated KEGG pathways (Figure 6c, Table S13). We also used the network-creating function of iDEP to identify clusters of related pathways and observed clusters related to proteasome, ribosome, and protein processing in the ER among the biological process and molecular function networks (FDR < 0.05) (Figure S15).

Previously, the ferrroptosis inducers erastin and sorabfenib, which inhibit system x_c^-, were found to induce significant ER stress and the activation of the unfolded protein response.[65,70] Therefore, we investigated whether the genes associated with ER stress and unfolded protein responses were upregulated in the treatment with CLA 18:3 compared to the control. Indeed, we observed a significant upregulation of *HSPA5* (p_{adj} = 0, fold change = 2.4) encoding for HSP70 chaperone BiP, the master regulator of the unfolded protein response.[71] In addition, genes associated with the PERK/EIF2a/ATF4 branch of the unfolded protein response, including *DDIT4* (p_{adj} = 3.31 × 10^{-39}, fold change = 5.39), *DDIT3* (p_{adj} = 1.29 × 10^{-23}, fold change = 3.66), and *CHAC1* (p_{adj} = 1.30 × 10^{-26}, fold change = 3.61) were significantly upregulated upon the addition of CLA 18:3.[72−74] Additionally, we further examined the expression patterns of the significant DEGs in CLA 18:3-treated cells by utilizing the Database for Annotation, Visualization and Integrated Discovery (DAVID) web server,[75] which identified the gene cluster related to unfolded protein response in the ER as the most enriched subset of genes with an enrichment score of 3.62 (Table S14). Together, the pathway analyses with iDEP, iPG, and DAVID suggest that CLA 18:3 in HT-1080 cell line leads to increased protein damage and ER stress relative to the control.

Furthermore, we used the upstream regulator analysis module of iPG to examine transcriptional regulators of gene expression and identified M-phase protein 6 (MPHOSPH6), C1D nuclear receptor corepressor (C1D), and DIS3 homologue, exosome endoribonuclease and 3′-5′ exoribonuclease (DIS3) as the most significantly activated upstream regulators in the CLA 18:3 versus control comparison (Figure 6e). This prediction was based on combined *p*-values (2.23 × 10^{-17}, 2.23 × 10^{-17}, and 3.55 × 10^{-17} for MPHOSPH6, C1D, and DIS3, respectively), which were calculated based on the number of DEGs supporting the hypothesis that the regulator is activated and the total number of DEGs downstream of the regulator. Interestingly, MPHOSPH6, C1D, and DIS3 activated similar DEG targets, which are the genes encoded for large ribosomal subunits (Figure 6h, Table S15, only the gene targets of MPHOSPH6 are shown). In addition, the following three most significantly activated upstream regulators in the CLA 18:3 versus control comparison, including eukaryotic translation initiation factor 5 (EIF5) (p = 1.85 × 10^{-10}), casein kinase 1 epsilon (CSNK1E) (p = 6.27 × 10^{-10}), and BUD23 rRNA methyltransferase and ribosome maturation factor (BUD23) (p = 1.05 × 10^{-09}), also activated similar targets, which are small ribosomal subunit-encoded genes (Figure 6i and Table S16, only the gene targets of EIF5 are shown).

We then compared the RNA-seq results between CLA 18:2 versus control and LA versus control comparisons and between RSL3-CLA 18:2 versus control and RSL3-LA versus control comparisons. Overall, the treatment with LA only or RSL3-LA only led to significant changes in 46 and 69 DEGs compared to the control (adjusted *p*-value <0.05, > 2-fold change), respectively (Figure 6b). Therefore, we focus on the comparison between the RSL3-CLA 18:2 the RSL3-LA groups. Among the significant DEGs identified in RSL3-CLA 18:2- and RSL3-LA-treated cells, only 43 genes were coregulated by both treatment groups, while 136 and 378 genes were uniquely regulated by RSL3-CLA 18:2 and RSL3-LA, respectively. Notably, pathway analyses of DEGs of the RSL3-CLA 18:2 versus control comparison using iDEP and iPG identified two

https://doi.org/10.1021/jacsau.2c00681
JACS Au 2023, 3, 1100−1117

significantly activated KEGG pathways, which are protein processing in the ER and proteasome (Figure 6d, Table S13). On the other hand, no significantly altered pathways were identified by the RSL3-LA versus control comparison. Moreover, MPHOSPH6, C1D, and DIS3 were also identified as the most activated upstream regulators in both treatments with RSL3-CLA 18:2 and RSL3-LA. However, the level of activation of these regulators was much more significant in the RSL3-CLA18:2 versus control comparison compared to the RSL3-LA versus control comparison. Specifically, in the RSL3-CLA18:2 versus control comparison, the combined p-values of MPHOSPH6, C1D, and DIS3 are 1.11×10^{-05}, 1.11×10^{-05}, and $5.14 \times 10^{-0}.5$ (FDR-corrected), respectively. In contrast, in the RSL3-LA versus control comparison, the FDR-corrected combined p-values of MPHOSPH6 and C1D are only 0.029 for both, and the activation of DIS3 is statistically insignificant with the combined p-value of 0.10. Furthermore, the subset of genes related to unfolded protein response in the ER was identified in RLS3-CLA 18:2-treated cells by DAVID functional clustering analysis with an enrichment score of 1.56 (Table S13), but not in the RLS3-LA-treated cells. In addition, despite not inducing cell death at 80 μM, CLA 18:2 alone coregulates 213 genes with CLA 18:3 (Figure S16). Among these coregulated genes, pathway analysis with DAVID identified genes associated with unfolded protein response as the most enriched subset of genes with an enrichment score of 4.15 (Table S17). Therefore, the pathway analyses of the RNA-seq data suggest that protein damage is more significant when treated with conjugated PUFAs than their nonconjugated counterparts.

DISCUSSION

This study aimed to investigate the relationship between the autoxidation reactivity and mechanisms of biologically important lipids to their biological effects. We found that 7-DHC, vitamin D_3, and retinal are highly toxic to cancer cells (Table S1). However, when used at their nonlethal concentrations, all these lipids potently inhibited cell death triggered by the ferroptosis inducers, including IKE and RSL3 (Figure 1, Table S2). While the antiferroptotic properties of 7-DHC, vitamin D_3, and the precursor of vitamin A, β-carotene, were previously demonstrated,[76−80] to our knowledge, this is the first study that reports the inhibition of ferroptosis by the two forms of vitamin A including retinol and retinal. Previously, vitamin A was reported to function as either a pro-oxidant or an antioxidant, depending on oxygen tension in the tissues or organs.[81−84] Here, vitamin A appeared to function as an antioxidant and a ferroptosis inhibitor.

The observed antiferroptotic properties of 7-DHC, vitamin D_3, and vitamin A highlight the importance of lipid incorporation into the cellular phospholipids to the ferroptosis induction. Specifically, during the initiation of ferroptosis, fatty acids are activated and incorporated into the membrane phospholipids via the enzymes such as LPCAT3 and ACSL4.[29,85,86] Since 7-DHC, vitamin D_3, and vitamin A do not undergo such processes, at nonlethal concentrations, they can potentially "hijack" the free radical chain reaction away from the membrane phospholipids due to their high reactivity toward lipid peroxidation with autoxidation (propagation) rate constants of 2737, 1031, 5656 M^{-1} s^{-1}, respectively,[14] making them much more reactive than the endogenous esterified PUFAs. Indeed, 7-DHC was recently shown to inhibit phospholipid autoxidation and, subsequently, ferroptosis.[76] Interestingly, the reduced form of another biologically important lipid, vitamin K, which shares similar structural properties with CoQ10, was recently found to be antiferroptotic.[87] Thus, these reactive biologically important lipids represent a class of natural compounds that can act as ferroptosis suppressors.

Nonconjugated PUFAs have been the focus of studies on ferroptosis in the literature,[24,29,44] but it was only recently that conjugated PUFAs, CLA 18:3 isomers α-eleostearic acid and pucinic acid, were shown to be proferroptotic,[31,32] even though the anticancer properties of various conjugated PUFAs have been previously recognized.[33,34,88−90] We confirmed CLA 18:3-induced cell death to be ferroptosis (Figure 2). Notably, different CLA 18:3 isomers were shown to induce ferroptosis without the addition of any ferroptosis-inducing compounds in this and previous studies,[31,32] which has not been observed with nonconjugated PUFAs. In addition, the CLA 18:3 isomer, α-eleostearic acid, was reported to induce ferroptosis without directly inhibiting GPX4 or affecting total cellular glutathione levels,[31] suggesting that it acts as a noncanonical ferroptosis inducer. We postulate that the large autoxidation rate constant of 1235 M^{-1} s^{-1} and the high level of toxic lipid electrophiles formed from the PRA mechanism for CLA 18:3 overwhelm the detoxification function of antioxidant enzymes such as GPX4 and FSP1 and, eventually, lead to cell death.

We also showed in this study that while displaying low toxicity when administered by itself, CLA 18:2 much more potently increased RSL3-induced toxicity than any other nonconjugated PUFAs in the HT-1080 cell line (Table S2). The difference in potency of CLA 18:2 and nonconjugated PUFAs can, in part, be attributed to their difference in autoxidation mechanism and kinetics. Specifically, CLA 18:2 undergoes autoxidation via both HAT and PRA mechanisms, with rate constants of 57 and 61 M^{-1} s^{-1}, respectively, while nonconjugated PUFAs do not have any contribution from the PRA mechanism, suggesting that the PRA mechanism or the resulting products more potently induce ferroptosis. Overall, these results suggest that the unusually high reactivity toward the PRA mechanism of conjugated PUFAs is underlying their high potency in enhancing ferroptosis compared to their nonconjugated counterparts.

The lipidomic results suggest that distinct cellular organelles and pathways are involved in the activation and incorporation of LA and CLA 18:2 into neutral lipids and phospholipids. For example, while the addition of LA led to a moderate increase in the levels of various TAG species, the addition of CLA 18:2 led to a much larger increase in specific TAGs (Figure 3c), especially 54:6 TAG (18:2/18:2/18:2), suggesting the potential accumulation of lipid droplets, which is consistent with the previous report.[31] We indeed observed the upregulation of TAG biosynthesis genes encoding glycerol-3-phosphate O-acyltransferase 3 (*GPAT3*) and phosphatidic acid phosphatase (*PLPP2* and *PLPP5*)[91] in CLA 18:2-treated samples (Table S19). The modulatory role of lipid droplets in ferroptosis is still under debate. Specifically, lipid droplets have been regarded as an antioxidant organelle that can sequester PUFAs away from the membrane and protect cells from oxidative damage and ferroptosis.[92−94] On the other hand, lipid droplets can act as a reservoir that supplies PUFAs for membrane phospholipid synthesis.[95] Indeed, the accumulation of PUFA-containing TAGs in lipid droplets, which can be catalyzed by ACSL1 or ACSL3, was shown to increase cell susceptibility to ferroptosis.[31,38,96] In addition, it has been

https://doi.org/10.1021/jacsau.2c00681
JACS Au 2023, 3, 1100−1117

suggested that lipid droplets accumulate during the early stage of ferroptosis but break down as cell death progresses, leading to an increase in PUFA-containing membrane phospholipids and promoting ferroptosis sensitivity.[97,98] Furthermore, lipid droplet viscosity was shown to increase during erastin- and RSL3-induced ferroptosis in different cancer cell lines while remaining the same in the cotreatment of erastin and Fer-1,[99] suggesting an increase in oxidized PUFAs in lipid droplets during ferroptosis. Thus, lipid droplets can potentially be additional sites where lipid peroxidation happens. Therefore, we postulate that the accumulation of highly oxidizable conjugated PUFAs into TAGs can lead to lipid peroxidation within lipid droplets, contributing to ferroptosis sensitivity. Further investigation is necessary to elucidate whether the accumulations of conjugated PUFAs into neutral lipids and lipid droplets are essential for conjugated PUFA-induced ferroptosis.

Interestingly, we found that the addition of CLA 18:2 led to a significant increase in the normalized abundance of long-chain and highly unsaturated ether phospholipids, while the levels of these lipids were not significantly altered in LA-treated cells (Figure 3d,e). This is important because ether phospholipids and their peroxisome-driven biosynthesis were also shown to promote ferroptosis recently.[52,53,100] Furthermore, we observed the incorporation of fatty acid 18:2 into the *sn*-1 position of the significantly elevated ether-PEs, suggesting the involvement of peroxisome in facilitating the incorporation of exogenous CLA 18:2 into ether lipids (Figure S6d−f). This is in contrast with the findings by Zou et al. that the PUFA moiety, not the alkenyl ether group, which contained the nonoxidizable fatty acid 18:0 in that study, on plasmalogens is essential in potentiating ferroptosis.[52] The biosynthesis of ether lipids starts in peroxisome, where fatty acids are activated into acyl-CoA, reduced into fatty alcohol, which was then used to displace the acyl chain of the *sn*-1 position of acyl-dihydroxyacetone, the precursor of ether lipid synthesis.[101] The exchange of the acyl chain for an alkyl group leading to the formation of the ether bond at the *sn*-1 position is the rate-limiting step in ether lipid biosynthesis and is facilitated by alkylglycerone phosphate synthase (AGPS). It should be noted that the role of AGPS-dependent ether lipid synthesis in ferroptosis was recently reported to be only context-dependent since the disruption of this process was found to have little effect on erastin2- or RSL3-induced cell death.[102] Therefore, the synthesis of ether lipids may be more relevant to the lethality of RSL3-CLA 18:2 cotreatment, which distinguishes the lethal mechanism potentiated by exogenous conjugated PUFAs from cell death induced by the canonical ferroptosis inducers. Further investigation is necessary to elucidate the importance of ether lipid biosynthesis in conjugated PUFA-induced ferroptosis.

Compared to the oxidation of LA, the oxidation of CLA 18:2 led to much more complex oxidation product profiles (Figure S9), owing to the contribution of both the HAT and PRA mechanisms to the propagation step. Here, we proposed a mechanism of PRA to the conjugated double bonds of CLA 18:2 and CLA 18:3 that accounts for the formation of peroxide dimers and polymers (Figures 4a and S10) and subsequently α,β-unsaturated aldehydes, such as 2-*t*-octenal from CLA 18:2 and 2,4-*tt*-nonadienal from CLA 18:3 (Figure 4a,b). We validated this mechanism by the confirmation of the formation of these aldehydes using DNPH trapping. Importantly, higher levels of electrophilic aldehydes were formed from the oxidation of conjugated PUFAs than nonconjugated PUFAs.

We then showed that the unsaturated aldehydes, including 2-octenal, 2-*t*-nonenal, and 2,4-*tt*-nonadienal, detected from the oxidation of conjugated PUFAs are highly toxic in HT-1080 cell lines (Table S12). Terminal unsaturated aldehydes are highly electrophilic and can lead to significant protein modifications via Michael adduction at cysteine, histidine, and lysine residues and Schiff base formation at lysine residue. Indeed, reactions between proteins and 2-octenal were previously reported to result in significant losses of histidine and lysine residues.[103,104] In addition, 2,4-*tt*-nonadienal can modify the protein side chains, leading to substantial protein structural alterations and aggregations.[105] In the context of ferroptosis, significant protein modifications by lipid-derived electrophiles were detected in HT-1080 cells treated with RSL3.[106] Furthermore, in addition to protein modifications, the execution phase of ferroptosis also involves pore formation in the plasma membrane, leading to increased cell swelling and calcium influx and, eventually, cell rupture.[107,108] Importantly, pore formation on lipid membrane was only observed for lipid-derived aldehydes, not lipid peroxides, owing to their shorter and highly mobile tails.[109] Together, these findings highlight the importance of lipid-derived electrophiles in the execution of ferroptosis. In fact, impaired detoxification of lipid-derived electrophiles was recently suggested to be a hallmark of ferroptosis.[110] Thus, we hypothesize that the accumulation of the highly toxic electrophilic aldehydes contributes to the high potency of conjugated PUFAs in potentiating ferroptosis. Indeed, pathway analysis from RNA-seq results suggests increased protein damage and ER stress in cells treated with conjugated PUFAs (Figure 6). Specifically, in conjugated PUFA-treated cells, we observed an upregulation of unfolded protein response (Table S13), indicating the accumulation of unfolded or misfolded protein in the ER, which was previously reported for highly toxic electrophiles such as 4-HNE.[64] These results suggest that ER is an important organelle in ferroptosis induced by conjugated PUFAs, which is consistent with the recent report that ER is an essential site of lipid peroxidation in ferroptosis.[111]

Unlike the nonconjugated PUFAs, which can be synthesized inside the cells, the conjugated PUFAs can only be obtained from meat and dairy products from ruminants and plant-based food products such as pomegranate seed oil and bitter gourd seed.[35,36,112,113] Therefore, our results highlight the potential of dietary PUFAs in improving the outcomes of ferroptosis inducers. For example, it has been suggested that dietary PUFAs can increase the sensitivity of tumor cells to $CD8^+$ T-cell ferroptosis-driving activity.[114] In addition, increased CD36-mediated exogenous PUFA uptake was recently shown in acidified cancer cells.[94] Therefore, highly reactive conjugated PUFAs, such as CLA 18:3, can potentially be utilized as therapeutics for tumors in acidic microenvironments.

METHODS

Cell Lines and Culture Conditions

HT-1080 and SK-N-SH cell lines were obtained from American Type Culture Collection (ATCC). 786-O cell line was a generous gift from the lab of Professor Rheem Totah. HT-1080 and SK-N-SH cell lines were grown in DMEM High-Glucose media (Gibco) containing 10% fetal bovine serum (FBS; Gibco), 1% MEM nonessential amino acids (Gibco), and 1% Penicillin-Streptomycin (Pen-Strep, 10,000 U/mL; Gibco). 786-O cell line was grown in RPMI-1640 media (Gibco)

https://doi.org/10.1021/jacsau.2c00681
JACS Au 2023, 3, 1100−1117

containing 10% FBS and 1% Pen-Strep. All cells were cultured in a humidified condition at 37 °C with 5% CO_2.

Chemicals

7-DHC, ferric citrate, iron chloride hexahydrate, ferric ammonium citrate, sulfate heptahydrate, a-tocopherol, deferoxamine mesylate salt, pentanal, hexanal, 2-*trans*-heptenal, 2-*trans*-octenal, 2-*trans*-nonenal, 2,4-*trans,trans*-hexadienal, 2,4-*trans,trans*-nonadienal, and 2,4-*trans,-trans*-decadienal were obtained from Sigma-Aldrich. Retinol, 2,4-dinitrophenylhydrazine (DNPH), and LpDNPH S10L cartridges were purchased from Thermo Fisher Scientific. Retinal, coenzyme Q_{10}, and vitamin D_3 were purchased from Chem-Impex Int'l Inc. Oleic acid (OA), linoleic acid (LA), 9,12,15-*cis,cis,cis*-octadecatrienoic acid (NLA 18:3), arachidonic acid (AA), eicosapentaenoic acid (EPA), docosahexaenoic acid (DHA), and 10,12-*trans,cis*-octadecadienoic acid (CLA 18:2) were purchased from Nu-Chek Prep, Inc. 9,11,13-*trans,trans,trans*-octadecatrienoic acid (CLA 18:3) was obtained from Sapphire North America. 1,2-dimyristoyl-*sn*-glycero-3-phosphocholine (DMPC) was obtained from Avanti Polar Lipids. Imidazole ketone erastin (IKE), RSL3, liproxstatin-1, and ferrostatin-1 were obtained from MedChemExpress. 4-hydroxynonenal (4-HNE) was purchased from Cayman Chemical. The radical initiator, MeOAMVN, was purchased from Wako Chemicals.

Cell Viability Assays

Cells were seeded in 96-well plates (Corning 3598) at 5000 cells/well and treated with indicated compounds 24 h after plating. Compounds are added at the same time in cotreatments. Cell viability was assessed using CellTiter 96 Aqueous One Solution Assay (Promega) according to the manufacturer's instructions. Viability was reported as percentages relative to vehicle control, and EC_{50} curves were generated with GraphPad Prism (version 9).

Analysis of Lipid Peroxidation Using Flow Cytometry

The experiment was conducted following the protocol described by Martinez et al.[115] Briefly, HT-1080 cells were seeded at 1.7×10^5 cells/well in a 6-well plate (Corning 3506). After 24 h, cells were treated with test compounds for the indicated times and then incubated with BODIPY 581/591 C11 (Invitrogen D3861) at 37 °C for 20 min. Stained cells were then washed with Hanks Balanced Salt Solution (HBSS; Gibco) and harvested by trypsinization. Harvested cells were resuspended in HBSS, strained through a 40 mm cell strainer, and analyzed by a flow cytometer (LSR II, BD Biosciences). Flow cytometry data was analyzed using FACSDiva software, and the plots were generated using FlowJo software.

Reduced Glutathione Measurement

Cells were seeded in 96-well plates at 5000 cells/well and treated with indicated concentrations of CLA 18:3 24 h after plating. After indicated treatment times, cellular reduced glutathione was measured using the GSH-Glo Glutathione Assay (Promega). CLA 18:3-treated samples were normalized to parallel cell viability measurements using CellTiter 96 Aqueous One Solution Assay (Promega).

Lipidomics Analysis

Triplicate samples of HT-1080 cells at ∼60% confluence were incubated with vehicle (DMSO), 5 nM RSL3, 80 μM LA, 5 nM RSL3 + 80 μM LA, 80 μM CLA 18:2, 5 nM RSL3 + 80 μM CLA 18:2, or 3 μM CLA 18:3 overnight. The cell pellets harvested were resuspended in cold PBS and lysed by sonication on ice for 30 min. Protein concentration was measured using the Bio-Rad DC protein mass assay. Lipids were extracted using the Folch method as previously described.[49] The extracted organic layer was transferred to a Pyrex glass centrifuge tube (Corning 99502−10) and dried in a speed vacuum concentrator (Thermo Fisher Savant). The dried lipid extracted was reconstituted in methylene chloride and stored at −80 °C until analysis.

Prior to analysis, 25 μL of the extract was transferred in LC vials, dried under argon, and reconstituted in 100 μL of 90% methanol in water with 0.1% formic acid. A pooled quality control sample was prepared by combining an equal volume from each final sample into a separate LC vial. Chromatographic separation was performed using a Waters Acquity FTN ultraperformance liquid chromatography (Waters Corp, Milford, Massachusetts) with a hydrophilic interaction column (HILIC; Phenomenex Kinetex, 100 × 2.1 mm, 1.7 μm) maintained at 40 °C at a flow rate of 0.5 mL/min. A sample injection volume of 5 μL was used for both positive and negative mode analyses. Mobile phase A consisted of acetonitrile/water (50:50, v/v) and mobile phase B was acetonitrile/water (95:5, v/v/v), both containing 5 mM ammonium acetate. The linear gradient was as follows: 0−1 min, 100% B; 4 min, 90% B; 7−8 min, 70% B; 9−12 min, 100% B.

Ion mobility-mass spectrometry (IM-MS) analysis was performed on the Waters Synapt G2-XS platform in both positive and negative modes. Capillary voltages of +3.0 and −2.0 kV were used for positive and negative modes, respectively. Other ESI conditions were as follows: sampling cone, 40 V; extraction cone, 80 V; source temperature, 100 °C; desolvation temperature, 350 °C; cone gas,10 L/h; and desolvation gas, 1000 L/h. Mass calibration over m/z 50−1200 was performed with sodium formate. Collision cross-section calibration was performed as previously described.[49] IM separation was performed with a traveling wave velocity of 500 m/s and wave height of 40 V. Data was acquired for m/z 50−1200 with a 0.5 s scan time. Leucine enkephalin was acquired as a lockspray signal for postacquisition correction of mass and drift time.

Data alignment, peak detection, and normalization were performed in Progenesis QI (Nonlinear Dynamics). The chromatographic region between 0.4 and 8.5 min was considered for peak detection. The prepared pooled QC sample was used as the reference sample for alignment, and data were normalized to all compounds. The resulting data set was filtered by analysis of variance (ANOVA) p-value < 0.05. Principal components and additional multivariate statistical analyses were performed in EZInfo (Umetrics). Lipid identifications were made based on m/z (within 0.01 Da mass accuracy), retention time (within 0.3 min accuracy), and CCS (within 3.0 $Å^2$ accuracy), using LiPydomics.[50] Only lipid identifications that satisfied all three levels of identification, including m/z, retention time, and CCS, were considered. Data are presented as mean ± standard deviation. Statistical analyses relative to control were conducted using Student's t test assuming unequal variance with a Bonferroni correction for multiple comparisons

Lipids of interest for MS/MS fragmentation were selected based on two criteria: (1) the lipids have normalized abundance over 8000 in the treatment group and (2) the fold change in normalized abundance in the treatment group compared to the control is at least 2. The targeted MS/MS fragmentation m/z was performed in the transfer region with a collision energy ramp of 25−40 V with 0.2 s scan time. The fragmentation and composition of lipids were confirmed using LIPID MAPS Structure Database.

Detection of DNPH-Derivatized Aldehydes Using Reverse-Phase MS and MS/MS

Here 1 mL solutions of LA, CLA 18:2, and CLA 18:3 (as free fatty acid and as CLA18:3-containing TAGs in tung oil) in benzene at the same concentration (35.9 μM) were subjected to oxidation using 5% mol MeOAMVN at 37 °C for 2 h. The concentration for tung oil solution was calculated based on the assumption that 75% of tung oil content is CLA 18:3-containing TAG. The DNPH-derivatized aldehydes from the oxidation mixture were separated via reverse-phase chromatography with the following conditions: C18 column (Kinetex, 100 mm × 2.1 mm, 1.7 μm particle diameter; Phenomenex); flow rate, 0.3 mL/min; and gradient elution method with solvent A (water) and solvent B (methanol) was used: 0 min, 80% B; 9 min, 95% B; 12−15 min, 80% B. Untargeted MS and targeted MS/MS fragmentation analysis of the oxidation samples was performed on the Waters Synapt G2-XS platform in negative mode with 0.25 s scan time. Capillary voltage of −2.0 kV was used. Other ESI conditions were as follows: sampling cone, 40 V; extraction cone, 80 V; source temperature, 100 °C; desolvation temperature, 350 °C; cone gas,10 L/h; and desolvation gas, 1000 L/h. Mass calibration over m/z 50−1200 was performed with sodium formate. The commercially available aldehyde standards were also derivatized with DNPH and

https://doi.org/10.1021/jacsau.2c00681
JACS Au 2023, 3, 1100−1117

fragmented to obtain the reference spectrum and the optimal fixed collision energy for each DNPH-derivatized aldehyde. The transfer collision energy used for each aldehyde was as follows: pentanal, 15 V; hexanal, 11 V; 2-*t*-heptenal, 14 V; 2-*t*-octenal, 14 V; 2-*t*-nonenal, 15 V; 4-HNE, 16 V; 2,4-*tt*-hexadienal, 13 V; 2,4-*tt*-nonadienal, 16 V; and 2,4-*tt*-decadienal, 17. A pooled standard sample was prepared by combining each derivatized standard into a separate LC vial. Aldehyde identifications were made based on m/z, retention time, and fragmentation patterns of the targeted aldehyde from the pooled standards.

RNA Sequencing

Quadruplicate samples of HT-1080 cells at ∼60% confluence were incubated with vehicle (DMSO), 10 nM RSL3, 10 nM RSL3 + 80 μM LA, 10 nM RSL3 + 80 μM CLA 18:2, and 5 μM CLA 18:3 overnight. Total RNA was isolated from each sample using the RNeasy kit (Qiagen) and sent to Novogene to perform the cDNA library construction and sequencing using the Illumina NovaSeq 6000 platform (150 base pairs paired-end, with sequencing depth above 20 million reads per sample). Novogene confirmed the RNA integrity and purity using the Agilent 2100 BioAnalyzer (Agilent Technologies Inc.). All samples met Novogene requirements of library construction and were submitted for RNA sequencing. Raw RNA sequencing reads in FASTQ format were mapped to the human genome (hg38) using HISAT algorithm[116] and format conversions were performed using Samtools.[117] FeatureCounts algorithm was used to quantify the aligned RNA-seq data as raw counts.[118] The DESeq2 R package was used to determine DEGs from raw counts in different conditions.[119]

■ ASSOCIATED CONTENT

Data Availability Statement

RNaseq data is available from the National Center for Biotechnology GEO database (GSE224249). The raw lipidomics data can be accessed at MassIVE (MSV000091187).

Supporting Information

The Supporting Information is available free of charge at https://pubs.acs.org/doi/10.1021/jacsau.2c00681.

Additional cell viability dose−response curves for SH-N-SK and 786-O cell lines, supplementary lipidomics data, MS and MS/MS traces, networks of Gene Ontology (GO) identified by iDEP analysis in HT-1080 cells treated with CLA 18:3 compared to the control; and supplementary tables for cytotoxicity of biologically important lipids and their effects on IKE and RSL3 cytotoxicity, altered lipids in HT-1080 cells exposed to CLA 18:2, LA, and CLA 18:3 in both positive and negative modes, area under the curve for each aldehyde from the oxidation of CLA 18:2 vs LA, cytotoxicity of different aldehydes, and pathway analyses in cells treated with conjugated PUFAs (PDF)

Gene list from RNAseq analysis of CLA 18:3 vs control (XLSX)

Gene list from RNAseq analysis of CLA 18:2+RSL3 vs control (XLSX)

Gene list from RNAseq analysis of LA+RSL3 vs control (XLSX)

■ AUTHOR INFORMATION

Corresponding Author

Libin Xu − *Department of Medicinal Chemistry, University of Washington, Seattle, Washington 98195, United States;* orcid.org/0000-0003-1021-5200; Phone: (206) 543-1080; Email: libinxu@uw.edu; Fax: (206) 685-3252

Authors

Quynh Do − *Department of Medicinal Chemistry, University of Washington, Seattle, Washington 98195, United States*

Rutan Zhang − *Department of Medicinal Chemistry, University of Washington, Seattle, Washington 98195, United States*

Gavin Hooper − *Department of Medicinal Chemistry, University of Washington, Seattle, Washington 98195, United States*

Complete contact information is available at: https://pubs.acs.org/10.1021/jacsau.2c00681

Author Contributions

Quynh Do: data curation, formal analysis, investigation, methodology, validation, visualization, writing−original draft, writing−review and editing. Rutan Zhang: data curation, formal analysis, investigation, methodology, writing−review and editing. Gavin Hooper: data curation, formal analysis, investigation, writing−review and editing. Libin Xu: conceptualization, formal analysis, funding acquisition, investigation, project administration, supervision, writing−review and editing.

Notes

The authors declare no competing financial interest.

■ ACKNOWLEDGMENTS

This work is supported by grants from the National Science Foundation (CHE-1664851) and the National Institutes of Health (R01HD092659). We thank the assistance of Dr. Theo Bammler for the analysis of RNAseq data using iPathwayGuide at the UW Interdisciplinary Center for Exposures, Diseases, Genomics and Environment, which is supported by the NIH grant P30ES007033.

■ REFERENCES

(1) Ray, P. D.; Huang, B. W.; Tsuji, Y. Reactive oxygen species (ROS) homeostasis and redox regulation in cellular signaling. *Cell Signal* **2012**, *24* (5), 981−90.

(2) Yin, H.; Xu, L.; Porter, N. A. Free Radical Lipid Peroxidation: Mechanisms and Analysis. *Chem. Rev.* **2011**, *111* (10), 5944−5972.

(3) Davì, G.; Falco, A.; Patrono, C. Lipid peroxidation in diabetes mellitus. *Antioxid. Redox Signal.* **2005**, *7* (1−2), 256−68.

(4) Ames, B. N. DNA damage from micronutrient deficiencies is likely to be a major cause of cancer. *Mutat. Res.* **2001**, *475* (1−2), 7−20.

(5) Barrera, G. Oxidative stress and lipid peroxidation products in cancer progression and therapy. *ISRN Oncol* **2012**, *2012*, 137289.

(6) Spiteller, G. The important role of lipid peroxidation processes in aging and age dependent diseases. *Mol. Biotechnol* **2007**, *37* (1), 5−12.

(7) Simonian, N. A.; Coyle, J. T. Oxidative stress in neurodegenerative diseases. *Annu. Rev. Pharmacol Toxicol* **1996**, *36*, 83−106.

(8) Sayre, L. M.; Zelasko, D. A.; Harris, P. L.; Perry, G.; Salomon, R. G.; Smith, M. A. 4-Hydroxynonenal-derived advanced lipid peroxidation end products are increased in Alzheimer's disease. *J. Neurochem.* **1997**, *68* (5), 2092−7.

(9) Helberg, J.; Pratt, D. A. Autoxidation. *Chem. Soc. Rev.* **2021**, *50* (13), 7343−7358.

(10) Xu, L.; Porter, N. A. Free radical oxidation of cholesterol and its precursors: Implications in cholesterol biosynthesis disorders. *Free Radic Res.* **2015**, *49* (7), 835−849.

(11) Porter, N. A.; Xu, L.; Pratt, D. A. Reactive Sterol Electrophiles: Mechanisms of Formation and Reactions with Proteins and Amino Acid Nucleophiles. *Chemistry (Basel)* **2020**, *2* (2), 390−417.
(12) Liu, W.; Porter, N. A.; Schneider, C.; Brash, A. R.; Yin, H. Formation of 4-hydroxynonenal from cardiolipin oxidation: Intramolecular peroxyl radical addition and decomposition. *Free Radic Biol. Med.* **2011**, *50* (1), 166−178.
(13) Xu, L.; Korade, Z.; Rosado, D. A., Jr; Liu, W.; Lamberson, C. R.; Porter, N. A. An oxysterol biomarker for 7-dehydrocholesterol oxidation in cell/mouse models for Smith-Lemli-Opitz syndrome. *J. Lipid Res.* **2011**, *52* (6), 1222−33.
(14) Do, Q.; Lee, D. D.; Dinh, A. N.; Seguin, R. P.; Zhang, R.; Xu, L. Development and Application of a Peroxyl Radical Clock Approach for Measuring Both Hydrogen-Atom Transfer and Peroxyl Radical Addition Rate Constants. *J. Org. Chem.* **2021**, *86* (1), 153−168.
(15) Dixon, S. J.; Lemberg, K. M.; Lamprecht, M. R.; Skouta, R.; Zaitsev, E. M.; Gleason, C. E.; Patel, D. N.; Bauer, A. J.; Cantley, A. M.; Yang, W. S.; Morrison, B., 3rd; Stockwell, B. R. Ferroptosis: an iron-dependent form of nonapoptotic cell death. *Cell* **2012**, *149* (5), 1060−72.
(16) Yang, W. S.; Stockwell, B. R. Ferroptosis: Death by Lipid Peroxidation. *Trends Cell Biol.* **2016**, *26* (3), 165−176.
(17) Stockwell, B. R. Ferroptosis turns 10: Emerging mechanisms, physiological functions, and therapeutic applications. *Cell* **2022**, *185* (14), 2401−2421.
(18) Szatrowski, T. P.; Nathan, C. F. Production of Large Amounts of Hydrogen Peroxide by Human Tumor Cells. *Cancer Res.* **1991**, *51* (3), 794.
(19) Yang, W. S.; SriRamaratnam, R.; Welsch, M. E.; Shimada, K.; Skouta, R.; Viswanathan, V. S.; Cheah, J. H.; Clemons, P. A.; Shamji, A. F.; Clish, C. B.; Brown, L. M.; Girotti, A. W.; Cornish, V. W.; Schreiber, S. L.; Stockwell, B. R. Regulation of ferroptotic cancer cell death by GPX4. *Cell* **2014**, *156* (1−2), 317−331.
(20) Seibt, T. M.; Proneth, B.; Conrad, M. Role of GPX4 in ferroptosis and its pharmacological implication. *Free Radical Biol. Med.* **2019**, *133*, 144−152.
(21) Friedmann Angeli, J. P.; Schneider, M.; Proneth, B.; Tyurina, Y. Y.; Tyurin, V. A.; Hammond, V. J.; Herbach, N.; Aichler, M.; Walch, A.; Eggenhofer, E.; Basavarajappa, D.; Rådmark, O.; Kobayashi, S.; Seibt, T.; Beck, H.; Neff, F.; Esposito, I.; Wanke, R.; Förster, H.; Yefremova, O.; Heinrichmeyer, M.; Bornkamm, G. W.; Geissler, E. K.; Thomas, S. B.; Stockwell, B. R.; O'Donnell, V. B.; Kagan, V. E.; Schick, J. A.; Conrad, M. Inactivation of the ferroptosis regulator Gpx4 triggers acute renal failure in mice. *Nat. Cell Biol.* **2014**, *16* (12), 1180−91.
(22) Doll, S.; Freitas, F. P.; Shah, R.; Aldrovandi, M.; da Silva, M. C.; Ingold, I.; Goya Grocin, A.; Xavier da Silva, T. N.; Panzilius, E.; Scheel, C. H.; Mourão, A.; Buday, K.; Sato, M.; Wanninger, J.; Vignane, T.; Mohana, V.; Rehberg, M.; Flatley, A.; Schepers, A.; Kurz, A.; White, D.; Sauer, M.; Sattler, M.; Tate, E. W.; Schmitz, W.; Schulze, A.; O'Donnell, V.; Proneth, B.; Popowicz, G. M.; Pratt, D. A.; Angeli, J. P. F.; Conrad, M. FSP1 is a glutathione-independent ferroptosis suppressor. *Nature* **2019**, *575* (7784), 693−698.
(23) Bersuker, K.; Hendricks, J. M.; Li, Z.; Magtanong, L.; Ford, B.; Tang, P. H.; Roberts, M. A.; Tong, B.; Maimone, T. J.; Zoncu, R.; Bassik, M. C.; Nomura, D. K.; Dixon, S. J.; Olzmann, J. A. The CoQ oxidoreductase FSP1 acts parallel to GPX4 to inhibit ferroptosis. *Nature* **2019**, *575* (7784), 688−692.
(24) Yang, W. S.; Kim, K. J.; Gaschler, M. M.; Patel, M.; Shchepinov, M. S.; Stockwell, B. R. Peroxidation of polyunsaturated fatty acids by lipoxygenases drives ferroptosis. *Proc. Natl. Acad. Sci. U. S. A.* **2016**, *113* (34), No. E4966.
(25) Jiang, X.; Stockwell, B. R.; Conrad, M. Ferroptosis: mechanisms, biology and role in disease. *Nat. Rev. Mol. Cell Biol.* **2021**, *22* (4), 266−282.
(26) Shah, R.; Shchepinov, M. S.; Pratt, D. A. Resolving the Role of Lipoxygenases in the Initiation and Execution of Ferroptosis. *ACS Central Science* **2018**, *4* (3), 387−396.
(27) Stockwell, B. R.; Jiang, X. The Chemistry and Biology of Ferroptosis. *Cell Chem. Biol.* **2020**, *27* (4), 365−375.
(28) Stockwell, B. R.; Jiang, X.; Gu, W. Emerging Mechanisms and Disease Relevance of Ferroptosis. *Trends Cell Biol.* **2020**, *30* (6), 478−490.
(29) Kagan, V. E.; Mao, G.; Qu, F.; Angeli, J. P.; Doll, S.; Croix, C. S.; Dar, H. H.; Liu, B.; Tyurin, V. A.; Ritov, V. B.; Kapralov, A. A.; Amoscato, A. A.; Jiang, J.; Anthonymuthu, T.; Mohammadyani, D.; Yang, Q.; Proneth, B.; Klein-Seetharaman, J.; Watkins, S.; Bahar, I.; Greenberger, J.; Mallampalli, R. K.; Stockwell, B. R.; Tyurina, Y. Y.; Conrad, M.; Bayır, H. Oxidized arachidonic and adrenic PEs navigate cells to ferroptosis. *Nat. Chem. Biol.* **2017**, *13* (1), 81−90.
(30) Yamada, N.; Karasawa, T.; Kimura, H.; Watanabe, S.; Komada, T.; Kamata, R.; Sampilvanjil, A.; Ito, J.; Nakagawa, K.; Kuwata, H.; Hara, S.; Mizuta, K.; Sakuma, Y.; Sata, N.; Takahashi, M. Ferroptosis driven by radical oxidation of n-6 polyunsaturated fatty acids mediates acetaminophen-induced acute liver failure. *Cell Death Dis* **2020**, *11* (2), 144.
(31) Beatty, A.; Singh, T.; Tyurina, Y. Y.; Tyurin, V. A.; Samovich, S.; Nicolas, E.; Maslar, K.; Zhou, Y.; Cai, K. Q.; Tan, Y.; Doll, S.; Conrad, M.; Subramanian, A.; Bayır, H.; Kagan, V. E.; Rennefahrt, U.; Peterson, J. R. Ferroptotic cell death triggered by conjugated linolenic acids is mediated by ACSL1. *Nat. Commun.* **2021**, *12* (1), 2244.
(32) Vermonden, P.; Vancoppenolle, M.; Dierge, E.; Mignolet, E.; Cuvelier, G.; Knoops, B.; Page, M.; Debier, C.; Feron, O.; Larondelle, Y. Punicic Acid Triggers Ferroptotic Cell Death in Carcinoma Cells. *Nutrients* **2021**, *13* (8), 2751.
(33) Cornelius, A. S.; Yerram, N. R.; Kratz, D. A.; Spector, A. A. Cytotoxic Effect of *cis*-Parinaric Acid in Cultured Malignant Cells. *Cancer Res.* **1991**, *51* (22), 6025.
(34) Igarashi, M.; Miyazawa, T. Newly recognized cytotoxic effect of conjugated trienoic fatty acids on cultured human tumor cells. *Cancer Lett.* **2000**, *148* (2), 173−9.
(35) Suzuki, R.; Noguchi, R.; Ota, T.; Abe, M.; Miyashita, K.; Kawada, T. Cytotoxic effect of conjugated trienoic fatty acids on mouse tumor and human monocytic leukemia cells. *Lipids* **2001**, *36* (5), 477−82.
(36) Kohno, H.; Suzuki, R.; Noguchi, R.; Hosokawa, M.; Miyashita, K.; Tanaka, T. Dietary conjugated linolenic acid inhibits azoxymethane-induced colonic aberrant crypt foci in rats. *Jpn. J. Cancer Res.* **2002**, *93* (2), 133−42.
(37) Hassannia, B.; Wiernicki, B.; Ingold, I.; Qu, F.; Van Herck, S.; Tyurina, Y. Y.; Bayır, H.; Abhari, B. A.; Angeli, J. P. F.; Choi, S. M.; Meul, E.; Heyninck, K.; Declerck, K.; Chirumamilla, C. S.; Lahtela-Kakkonen, M.; Van Camp, G.; Krysko, D. V.; Ekert, P. G.; Fulda, S.; De Geest, B. G.; Conrad, M.; Kagan, V. E.; Vanden Berghe, W.; Vandenabeele, P.; Vanden Berghe, T. Nano-targeted induction of dual ferroptotic mechanisms eradicates high-risk neuroblastoma. *J. Clin Invest* **2018**, *128* (8), 3341−3355.
(38) Zou, Y.; Palte, M. J.; Deik, A. A.; Li, H.; Eaton, J. K.; Wang, W.; Tseng, Y. Y.; Deasy, R.; Kost-Alimova, M.; Dančík, V.; Leshchiner, E. S.; Viswanathan, V. S.; Signoretti, S.; Choueiri, T. K.; Boehm, J. S.; Wagner, B. K.; Doench, J. G.; Clish, C. B.; Clemons, P. A.; Schreiber, S. L. A GPX4-dependent cancer cell state underlies the clear-cell morphology and confers sensitivity to ferroptosis. *Nat. Commun.* **2019**, *10* (1), 1617.
(39) Xu, L.; Korade, Z.; Porter, N. A. Oxysterols from Free Radical Chain Oxidation of 7-Dehydrocholesterol: Product and Mechanistic Studies. *J. Am. Chem. Soc.* **2010**, *132* (7), 2222−2232.
(40) Korade, Z.; Xu, L.; Shelton, R.; Porter, N. A. Biological activities of 7-dehydrocholesterol-derived oxysterols: implications for Smith-Lemli-Opitz syndrome. *J. Lipid Res.* **2010**, *51* (11), 3259−69.
(41) Xu, L.; Mirnics, K.; Bowman, A. B.; Liu, W.; Da, J.; Porter, N. A.; Korade, Z. DHCEO accumulation is a critical mediator of pathophysiology in a Smith-Lemli-Opitz syndrome model. *Neurobiol. Dis.* **2012**, *45* (3), 923−929.
(42) Tomita, H.; Hines, K. M.; Herron, J. M.; Li, A.; Baggett, D. W.; Xu, L. 7-Dehydrocholesterol-derived oxysterols cause neurogenic defects in Smith-Lemli-Opitz syndrome. *eLife* **2022**, *11*, No. e67141.

https://doi.org/10.1021/jacsau.2c00681
JACS Au 2023, 3, 1100−1117

(43) Stockwell, B. R. A powerful cell-protection system prevents cell death by ferroptosis. *Nature* **2019**, *575* (7784), 597−598.
(44) Magtanong, L.; Ko, P. J.; To, M.; Cao, J. Y.; Forcina, G. C.; Tarangelo, A.; Ward, C. C.; Cho, K.; Patti, G. J.; Nomura, D. K.; Olzmann, J. A.; Dixon, S. J. Exogenous Monounsaturated Fatty Acids Promote a Ferroptosis-Resistant Cell State. *Cell Chem. Biol.* **2019**, *26* (3), 420−432.e9.
(45) Zitka, O.; Skalickova, S.; Gumulec, J.; Masarik, M.; Adam, V.; Hubalek, J.; Trnkova, L.; Kruseova, J.; Eckschlager, T.; Kizek, R. Redox status expressed as GSH:GSSG ratio as a marker for oxidative stress in paediatric tumour patients. *Oncol Lett.* **2012**, *4* (6), 1247−1253.
(46) Rebrin, I.; Sohal, R. S. Pro-oxidant shift in glutathione redox state during aging. *Adv. Drug Deliv Rev.* **2008**, *60* (13−14), 1545−52.
(47) Ghezzi, P. Regulation of protein function by glutathionylation. *Free Radic Res.* **2005**, *39* (6), 573−80.
(48) Li, A.; Hines, K. M.; Xu, L. Lipidomics by HILIC-Ion Mobility-Mass Spectrometry. In *Ion Mobility-Mass Spectrometry: Methods and Protocols*; Paglia, G., Astarita, G., Eds.; Springer US: New York, 2020; pp 119−132.
(49) Hines, K. M.; Herron, J.; Xu, L. Assessment of altered lipid homeostasis by HILIC-ion mobility-mass spectrometry-based lipidomics. *J. Lipid Res.* **2017**, *58* (4), 809−819.
(50) Ross, D. H.; Cho, J. H.; Zhang, R.; Hines, K. M.; Xu, L. LiPydomics: A Python Package for Comprehensive Prediction of Lipid Collision Cross Sections and Retention Times and Analysis of Ion Mobility-Mass Spectrometry-Based Lipidomics Data. *Anal. Chem.* **2020**, *92* (22), 14967−14975.
(51) Sindelar, P. J.; Guan, Z.; Dallner, G.; Ernster, L. The protective role of plasmalogens in iron-induced lipid peroxidation. *Free Radic Biol. Med.* **1999**, *26* (3−4), 318−24.
(52) Zou, Y.; Henry, W. S.; Ricq, E. L.; Graham, E. T.; Phadnis, V. V.; Maretich, P.; Paradkar, S.; Boehnke, N.; Deik, A. A.; Reinhardt, F.; Eaton, J. K.; Ferguson, B.; Wang, W.; Fairman, J.; Keys, H. R.; Dančík, V.; Clish, C. B.; Clemons, P. A.; Hammond, P. T.; Boyer, L. A.; Weinberg, R. A.; Schreiber, S. L. Plasticity of ether lipids promotes ferroptosis susceptibility and evasion. *Nature* **2020**, *585* (7826), 603−608.
(53) Cui, W.; Liu, D.; Gu, W.; Chu, B. Peroxisome-driven ether-linked phospholipids biosynthesis is essential for ferroptosis. *Cell Death Differ.* **2021**, *28* (8), 2536−2551.
(54) Roschek, B.; Tallman, K. A.; Rector, C. L.; Gillmore, J. G.; Pratt, D. A.; Punta, C.; Porter, N. A. Peroxyl Radical Clocks. *Journal of Organic Chemistry* **2006**, *71* (9), 3527−3532.
(55) Luna, P.; de la Fuente, M. A.; Salvador, D.; Márquez-Ruiz, G. Differences in Oxidation Kinetics between Conjugated and Non-conjugated Methyl Linoleate. *Lipids* **2007**, *42* (12), 1085−92.
(56) Suzuki, R.; Abe, M.; Miyashita, K. Comparative Study of the Autoxidation of TAG Containing Conjugated and Nonconjugated C 18 PUFA. *J. Amer Oil Chem. Soc.* **2004**, *81*, 563−569.
(57) Holman, R. T. Autoxidation of Fat and Related Substances. *Progress in the Chemistry of Fats and Other Lipid* **1954**, *2*, 51−98.
(58) Brimberg, U. I.; Kama-Eldin, A. On the kinetics of the autoxidation of fats: substrates with conjugated double bonds. *Eur. J. Lipid Sci. Technol.* **2003**, *105*, 17−22.
(59) García-Martínez, M. C.; Márquez-Ruiz, G.; Fontecha, J.; Gordon, M. H. Volatile Oxidation Compounds in a Conjugated Linoleic Acid-rich Oil. *Food Chem.* **2009**, *113*, 926−931.
(60) Kolliker, S.; Oehme, M.; Dye, C. Structure Elucidation of 2,4-Dinitrophenylhydrazone Derivatives of Carbonyl Compounds in Ambient Air by HPLC/MS and Multiple MS/MS Using Atmospheric Chemical Ionization in the Negative Ion Mode. *Anal. Chem.* **1998**, *70* (9), 1979−85.
(61) Berdyshev, E. V. Mass spectrometry of fatty aldehydes. *Biochim. Biophys. Acta* **2011**, *1811* (11), 680−93.
(62) Spiteller, G.; Kern, W.; Spiteller, P. Investigation of aldehydic lipid peroxidation products by gas chromatography-mass spectrometry. *Journal of Chromatography A* **1999**, *843* (1), 29−98.
(63) Shoeb, M.; Ansari, N. H.; Srivastava, S. K.; Ramana, K. V. 4-Hydroxynonenal in the pathogenesis and progression of human diseases. *Curr. Med. Chem.* **2013**, *21* (2), 230−7.
(64) Csala, M.; Kardon, T.; Legeza, B.; Lizák, B.; Mandl, J.; Margittai, E.; Puskás, F.; Száraz, P.; Szelényi, P.; Bánhegyi, G. On the role of 4-hydroxynonenal in health and disease. *Biochimica et Biophysica Acta (BBA) - Molecular Basis of Disease* **2015**, *1852* (5), 826−838.
(65) Dixon, S. J.; Patel, D. N.; Welsch, M.; Skouta, R.; Lee, E. D.; Hayano, M.; Thomas, A. G.; Gleason, C. E.; Tatonetti, N. P.; Slusher, B. S.; Stockwell, B. R. Pharmacological inhibition of cystine-glutamate exchange induces endoplasmic reticulum stress and ferroptosis. *Elife* **2014**, *3*, No. e02523.
(66) Nishizawa, H.; Matsumoto, M.; Shindo, T.; Saigusa, D.; Kato, H.; Suzuki, K.; Sato, M.; Ishii, Y.; Shimokawa, H.; Igarashi, K. Ferroptosis is controlled by the coordinated transcriptional regulation of glutathione and labile iron metabolism by the transcription factor BACH1. *J. Biol. Chem.* **2020**, *295* (1), 69−82.
(67) Ge, S. X.; Son, E. W.; Yao, R. iDEP: an integrated web application for differential expression and pathway analysis of RNA-Seq data. *BMC Bioinformatics* **2018**, *19* (1), 534.
(68) Ahsan, S.; Drăghici, S. Identifying Significantly Impacted Pathways and Putative Mechanisms with iPathwayGuide. *Current Protocols in Bioinformatics* **2017**, *57* (1), 7.15.1−7.15.30.
(69) Luo, W.; Friedman, M. S.; Shedden, K.; Hankenson, K. D.; Woolf, P. J. GAGE: generally applicable gene set enrichment for pathway analysis. *BMC Bioinformatics* **2009**, *10* (1), 161.
(70) Rahmani, M.; Davis, E. M.; Crabtree, T. R.; Habibi, J. R.; Nguyen, T. K.; Dent, P.; Grant, S. The kinase inhibitor sorafenib induces cell death through a process involving induction of endoplasmic reticulum stress. *Mol. Cell. Biol.* **2007**, *27* (15), 5499−513.
(71) Wang, J.; Lee, J.; Liem, D.; Ping, P. HSPA5 Gene encoding Hsp70 chaperone BiP in the endoplasmic reticulum. *Gene* **2017**, *618*, 14−23.
(72) Whitney, M. L.; Jefferson, L. S.; Kimball, S. R. ATF4 is necessary and sufficient for ER stress-induced upregulation of REDD1 expression. *Biochem. Biophys. Res. Commun.* **2009**, *379* (2), 451−5.
(73) Rozpedek, W.; Pytel, D.; Mucha, B.; Leszczynska, H.; Diehl, J. A.; Majsterek, I. The Role of the PERK/eIF2α/ATF4/CHOP Signaling Pathway in Tumor Progression During Endoplasmic Reticulum Stress. *Curr. Mol. Med.* **2016**, *16* (6), 533−44.
(74) Mungrue, I. N.; Pagnon, J.; Kohannim, O.; Gargalovic, P. S.; Lusis, A. J. CHAC1/MGC4504 is a novel proapoptotic component of the unfolded protein response, downstream of the ATF4-ATF3-CHOP cascade. *J. Immunol* **2009**, *182* (1), 466−76.
(75) Sherman, B. T.; Hao, M.; Qiu, J.; Jiao, X.; Baseler, M. W.; Lane, H. C.; Imamichi, T.; Chang, W. DAVID: a web server for functional enrichment analysis and functional annotation of gene lists (2021 update). *Nucleic Acids Res.* **2022**, *50* (W1), W216−21.
(76) Angeli, J. P. F.; Freitas, F. P.; Nepachalovich, P.; Puentes, L.; Zilka, O.; Inague, A.; Lorenz, S.; Kunz, V.; Nehring, H.; Silva, T. N. X. d.; Chen, Z.; Doll, S.; Schmitz, W.; Imming, P.; Miyamoto, S.; Klein-Seetharaman, J.; Kumar, L.; Genaro-Mattos, T. C.; Mirnics, K.; Meierjohann, S.; Kroiss, M.; Weigand, I.; Bommert, K.; Bargou, R.; Garcia-Saez, A.; Pratt, D.; Fedorova, M.; Wehmann, A.; Horling, A.; Bornkamm, G.; Conrad, M. 7-Dehydrocholesterol is an endogenous suppressor of ferroptosis. *Research Square*, October 6, 2021, ver. 1. DOI: 10.21203/rs.3.rs-943221/v1.
(77) Yamada, N.; Karasawa, T.; Komada, T.; Matsumura, T.; Baatarjav, C.; Ito, J.; Nakagawa, K.; Yamamuro, D.; Ishibashi, S.; Miura, K.; Sata, N.; Takahashi, M. DHCR7 as a novel regulator of ferroptosis in hepatocytes. *bioRxiv*, June 15, 2022, ver. 1. DOI: 10.1101/2022.06.15.496212.
(78) Liu, X.; Wang, S.; Jin, S.; Huang, S.; Liu, Y. Vitamin D3 attenuates cisplatin-induced intestinal injury by inhibiting ferroptosis, oxidative stress, and ROS-mediated excessive mitochondrial fission. *Food & Function* **2022**, *13* (19), 10210−10224.

(79) Cai, Y.; Li, X.; Tan, X.; Wang, P.; Zhao, X.; Zhang, H.; Song, Y. Vitamin D suppresses ferroptosis and protects against neonatal hypoxic-ischemic encephalopathy by activating the Nrf2/HO-1 pathway. *Translational Pediatrics* **2022**, *11*, 1633.
(80) Yagoda, N.; von Rechenberg, M.; Zaganjor, E.; Bauer, A. J.; Yang, W. S.; Fridman, D. J.; Wolpaw, A. J.; Smukste, I.; Peltier, J. M.; Boniface, J. J.; Smith, R.; Lessnick, S. L.; Sahasrabudhe, S.; Stockwell, B. R. RAS-RAF-MEK-dependent oxidative cell death involving voltage-dependent anion channels. *Nature* **2007**, *447* (7146), 864−8.
(81) Burton, G. W.; Ingold, K. U. beta-Carotene: an unusual type of lipid antioxidant. *Science* **1984**, *224* (4649), 569−73.
(82) Kennedy, T. A.; Liebler, D. C. Peroxyl radical scavenging by beta-carotene in lipid bilayers. Effect of oxygen partial pressure. *J. Biol. Chem.* **1992**, *267* (7), 4658−63.
(83) Palozza, P.; Calviello, G.; Bartoli, G. M. Prooxidant activity of beta-carotene under 100% oxygen pressure in rat liver microsomes. *Free Radic Biol. Med.* **1995**, *19* (6), 887−92.
(84) Tsuchihashi, H.; Kigoshi, M.; Iwatsuki, M.; Niki, E. Action of beta-carotene as an antioxidant against lipid peroxidation. *Arch. Biochem. Biophys.* **1995**, *323* (1), 137−47.
(85) Dixon, S. J.; Winter, G. E.; Musavi, L. S.; Lee, E. D.; Snijder, B.; Rebsamen, M.; Superti-Furga, G.; Stockwell, B. R. Human Haploid Cell Genetics Reveals Roles for Lipid Metabolism Genes in Nonapoptotic Cell Death. *ACS Chem. Biol.* **2015**, *10* (7), 1604−1609.
(86) Doll, S.; Proneth, B.; Tyurina, Y. Y.; Panzilius, E.; Kobayashi, S.; Ingold, I.; Irmler, M.; Beckers, J.; Aichler, M.; Walch, A.; Prokisch, H.; Trümbach, D.; Mao, G.; Qu, F.; Bayir, H.; Füllekrug, J.; Scheel, C. H.; Wurst, W.; Schick, J. A.; Kagan, V. E.; Angeli, J. P. F.; Conrad, M. ACSL4 dictates ferroptosis sensitivity by shaping cellular lipid composition. *Nat. Chem. Biol.* **2017**, *13* (1), 91−98.
(87) Mishima, E.; Ito, J.; Wu, Z.; Nakamura, T.; Wahida, A.; Doll, S.; Tonnus, W.; Nepachalovich, P.; Eggenhofer, E.; Aldrovandi, M.; Henkelmann, B.; Yamada, K.-i.; Wanninger, J.; Zilka, O.; Sato, E.; Feederle, R.; Hass, D.; Maida, A.; Mourão, A. S. D.; Linkermann, A.; Geissler, E. K.; Nakagawa, K.; Abe, T.; Fedorova, M.; Proneth, B.; Pratt, D. A.; Conrad, M. A non-canonical vitamin K cycle is a potent ferroptosis suppressor. *Nature* **2022**, *608* (7924), 778−783.
(88) Scimeca, J. A.; Thompson, H. J.; Ip, C. Effect of Conjugated Linoleic Acid on Carcinogenesis. In *Diet and Breast Cancer*; Weisburger, E. K., Ed.; Springer US: Boston, MA, 1994; pp 59−65.
(89) Dhar Dubey, K. K.; Sharma, G.; Kumar, A. Conjugated Linolenic Acids: Implication in Cancer. *J. Agric. Food Chem.* **2019**, *67* (22), 6091−6101.
(90) Tsuzuki, T.; Tokuyama, Y.; Igarashi, M.; Miyazawa, T. Tumor growth suppression by alpha-eleostearic acid, a linolenic acid isomer with a conjugated triene system, via lipid peroxidation. *Carcinogenesis* **2004**, *25* (8), 1417−25.
(91) Wilfling, F.; Wang, H.; Haas, J. T.; Krahmer, N.; Gould, T. J.; Uchida, A.; Cheng, J. X.; Graham, M.; Christiano, R.; Frohlich, F.; Liu, X.; Buhman, K. K.; Coleman, R. A.; Bewersdorf, J.; Farese, R. V., Jr; Walther, T. C. Triacylglycerol synthesis enzymes mediate lipid droplet growth by relocalizing from the ER to lipid droplets. *Dev Cell* **2013**, *24* (4), 384−99.
(92) Bailey, A. P.; Koster, G.; Guillermier, C.; Hirst, E. M.; MacRae, J. I.; Lechene, C. P.; Postle, A. D.; Gould, A. P. Antioxidant Role for Lipid Droplets in a Stem Cell Niche of Drosophila. *Cell* **2015**, *163* (2), 340−53.
(93) Jarc, E.; Kump, A.; Malavašič, P.; Eichmann, T. O.; Zimmermann, R.; Petan, T. Lipid droplets induced by secreted phospholipase A2 and unsaturated fatty acids protect breast cancer cells from nutrient and lipotoxic stress. *Biochimica et Biophysica Acta (BBA) - Molecular and Cell Biology of Lipids* **2018**, *1863* (3), 247−265.
(94) Dierge, E.; Debock, E.; Guilbaud, C.; Corbet, C.; Mignolet, E.; Mignard, L.; Bastien, E.; Dessy, C.; Larondelle, Y.; Feron, O. Peroxidation of n-3 and n-6 polyunsaturated fatty acids in the acidic tumor environment leads to ferroptosis-mediated anticancer effects. *Cell Metabolism* **2021**, *33* (8), 1701−1715.e5.
(95) Petan, T. Lipid Droplets in Cancer. *Reviews of Physiology, Biochemistry and Pharmacology* **2023**, *185*, 53.
(96) Klasson, T. D.; LaGory, E. L.; Zhao, H.; Huynh, S. K.; Papandreou, I.; Moon, E. J.; Giaccia, A. J. ACSL3 regulates lipid droplet biogenesis and ferroptosis sensitivity in clear cell renal cell carcinoma. *Cancer ; Metabolism* **2022**, *10* (1), 14.
(97) Tousignant, K. D.; Rockstroh, A.; Poad, B. L. J.; Talebi, A.; Young, R. S. E.; Taherian Fard, A.; Gupta, R.; Zang, T.; Wang, C.; Lehman, M. L.; Swinnen, J. V.; Blanksby, S. J.; Nelson, C. C.; Sadowski, M. C. Therapy-induced lipid uptake and remodeling underpin ferroptosis hypersensitivity in prostate cancer. *Cancer & Metabolism* **2020**, *8* (1), 11.
(98) Bai, Y.; Meng, L.; Han, L.; Jia, Y.; Zhao, Y.; Gao, H.; Kang, R.; Wang, X.; Tang, D.; Dai, E. Lipid storage and lipophagy regulates ferroptosis. *Biochem. Biophys. Res. Commun.* **2019**, *508* (4), 997−1003.
(99) Dong, B.; Song, W.; Lu, Y.; Sun, Y.; Lin, W. Revealing the Viscosity Changes in Lipid Droplets during Ferroptosis by the Real-Time and In Situ Near-Infrared Imaging. *ACS Sensors* **2021**, *6* (1), 22−26.
(100) Soula, M.; Weber, R. A.; Zilka, O.; Alwaseem, H.; La, K.; Yen, F.; Molina, H.; Garcia-Bermudez, J.; Pratt, D. A.; Birsoy, K. Metabolic determinants of cancer cell sensitivity to canonical ferroptosis inducers. *Nat. Chem. Biol.* **2020**, *16* (12), 1351−1360.
(101) Dean, J. M.; Lodhi, I. J. Structural and functional roles of ether lipids. *Protein & Cell* **2018**, *9* (2), 196−206.
(102) Magtanong, L.; Mueller, G. D.; Williams, K. J.; Billmann, M.; Chan, K.; Armenta, D. A.; Pope, L. E.; Moffat, J.; Boone, C.; Myers, C. L.; Olzmann, J. A.; Bensinger, S. J.; Dixon, S. J. Context-dependent regulation of ferroptosis sensitivity. *Cell Chemical Biology* **2022**, *29* (9), 1409−1418.
(103) Alaiz, M.; Beppu, M.; Ohishi, K.; Kikugawa, K. Modification of Delipidated Apoprotein B of Low Density Lipoprotein by Lipid Oxidation Products in Relation to Macrophage Scavenger Receptor Binding. *Biol. Pharm. Bull.* **1994**, *17* (1), 51−57.
(104) Alaiz, M.; Barragán, S. Reaction of a lysyl residue analogue with E-2-octenal. *Chem. Phys. Lipids* **1995**, *75* (1), 43−49.
(105) Dantas, L. S.; Viviani, L. G.; Inague, A.; Piccirillo, E.; Rezende, L. d.; Ronsein, G. E.; Augusto, O.; Medeiros, M. H. G.; Amaral, A. T. d.; Miyamoto, S. Lipid aldehyde hydrophobicity affects apo-SOD1 modification and aggregation. *Free Radical Biol. Med.* **2020**, *156*, 157−167.
(106) Chen, Y.; Liu, Y.; Lan, T.; Qin, W.; Zhu, Y.; Qin, K.; Gao, J.; Wang, H.; Hou, X.; Chen, N.; Friedmann Angeli, J. P.; Conrad, M.; Wang, C. Quantitative Profiling of Protein Carbonylations in Ferroptosis by an Aniline-Derived Probe. *J. Am. Chem. Soc.* **2018**, *140* (13), 4712−4720.
(107) Riegman, M.; Sagie, L.; Galed, C.; Levin, T.; Steinberg, N.; Dixon, S. J.; Wiesner, U.; Bradbury, M. S.; Niethammer, P.; Zaritsky, A.; Overholtzer, M. Ferroptosis occurs through an osmotic mechanism and propagates independently of cell rupture. *Nat. Cell Biol.* **2020**, *22* (9), 1042−1048.
(108) Pedrera, L.; Espiritu, R. A.; Ros, U.; Weber, J.; Schmitt, A.; Stroh, J.; Hailfinger, S.; von Karstedt, S.; García-Sáez, A. J. Ferroptotic pores induce Ca(2+) fluxes and ESCRT-III activation to modulate cell death kinetics. *Cell Death Differ.* **2021**, *28* (5), 1644−1657.
(109) Boonnoy, P.; Jarerattanachat, V.; Karttunen, M.; Wong-ekkabut, J. Bilayer Deformation, Pores, and Micellation Induced by Oxidized Lipids. *J. Phys. Chem. Lett.* **2015**, *6* (24), 4884−4888.
(110) Van Kessel, A. T. M.; Karimi, R.; Cosa, G. Live-cell imaging reveals impaired detoxification of lipid-derived electrophiles is a hallmark of ferroptosis. *Chemical Science* **2022**, *13* (33), 9727−9738.
(111) von Krusenstiern, A. N.; Robson, R. N.; Qian, N.; Qiu, B.; Hu, F.; Reznik, E.; Smith, N.; Zandkarimi, F.; Estes, V. M.; Dupont, M.; Hirschhorn, T.; Shchepinov, M. S.; Min, W.; Woerpel, K. A.; Stockwell, B. R. Identification of essential sites of lipid peroxidation in ferroptosis. *Nat. Chem. Biol.* **2023**, DOI: 10.1038/s41589-022-01249-3.
(112) Dhiman, T. R.; Anand, G. R.; Satter, L. D.; Pariza, M. W. Conjugated linoleic acid content of milk from cows fed different diets. *J. Dairy Sci.* **1999**, *82* (10), 2146−56.

(113) Destaillats, F.; Trottier, J. P.; Galvez, J. M.; Angers, P. Analysis of alpha-linolenic acid biohydrogenation intermediates in milk fat with emphasis on conjugated linolenic acids. *J. Dairy Sci.* **2005**, *88* (9), 3231−9.
(114) Stockwell, B. R.; Jiang, X. A Physiological Function for Ferroptosis in Tumor Suppression by the Immune System. *Cell Metabolism* **2019**, *30* (1), 14−15.
(115) Martinez, A. M.; Kim, A.; Yang, W. S. Detection of Ferroptosis by BODIPY 581/591 C11. *Methods Mol. Biol.* **2020**, *2108*, 125−130.
(116) Kim, D.; Langmead, B.; Salzberg, S. L. HISAT: a fast spliced aligner with low memory requirements. *Nat. Methods* **2015**, *12* (4), 357−360.
(117) Li, H.; Handsaker, B.; Wysoker, A.; Fennell, T.; Ruan, J.; Homer, N.; Marth, G.; Abecasis, G.; Durbin, R. The Sequence Alignment/Map format and SAMtools. *Bioinformatics* **2009**, *25* (16), 2078−9.
(118) Liao, Y.; Smyth, G. K.; Shi, W. featureCounts: an efficient general purpose program for assigning sequence reads to genomic features. *Bioinformatics* **2014**, *30* (7), 923−930.
(119) Love, M. I.; Huber, W.; Anders, S. Moderated estimation of fold change and dispersion for RNA-seq data with DESeq2. *Genome Biology* **2014**, *15* (12), 550.

https://doi.org/10.1021/jacsau.2c00681
JACS Au 2023, 3, 1100−1117